# Tracing Particles from the Sun to the Earth's Ionosphere

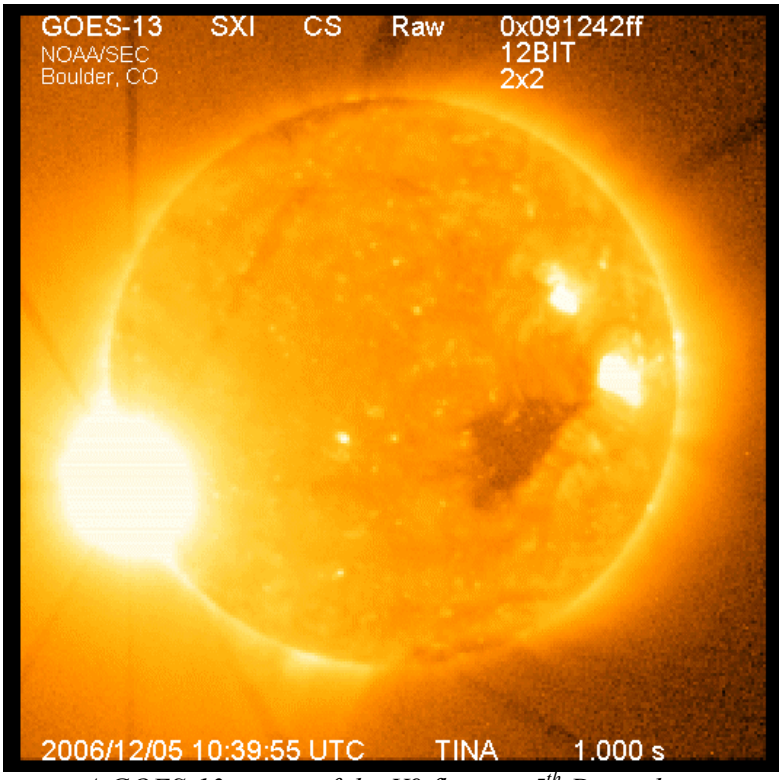


*A GOES-13 image of the X9 flare on 5th December.*

Sophie Murray
SS Astrophysics

# ABSTRACT

The aim of this project was to investigate the effect of solar activity on the Earth's ionosphere. An AWESOME (Atmospheric Weather Electromagnetic System for Observation Modelling and Education) antenna was constructed and used to monitor changes in the ionosphere. Changes were found to be caused by solar effects, as well as atmospherics.

1) Broadband data captured evidence of lightning strikes, also called sferics. From examination of the sferics' cut-off frequencies, ionospheric reflection heights were estimated to be 69.95 ± 11.90 km for during the day, and 86.48 ± 12.98 km for during the night. Electron densities were found to be in the region $10^2$ electrons/$cm^3$ at these heights.

2) Narrowband data showed typical changes in the ionosphere between night and day, with a higher signal at night in plots of amplitude vs. time, due to the disappearance of the D-layer, causing less attenuation. Sunrise and sunset times could be clearly seen in the plot, with a sharp decrease in amplitude during sunrise, and increase during sunset. From the sunrise times, an estimation of the terminator speed could be calculated for a number of days, all agreeing within limits of error to the theoretically calculated value of 276.87 m/s.

3) A number of solar X-flares were detected by the antenna, characterised by peaks in the amplitude plots. Electron densities in the ionosphere were found to increase due to the flares, by up to 67% in the case of the X9 flare of 5$^{th}$ December 2006.

# ACKNOWLEDGEMENTS

I would like to thank my supervisor, Dr. Peter Gallagher, for his continuing help on the project. Many thanks to Joe McAuley, for all his help in setting up the antenna. Thank you to those in the Mechanical Workshop, Mick in particular, for help with building the antenna. Thank you to Morris Cohen from Stanford University, for all his help with software problems, and invaluable troubleshooting advice. Also, thanks to the postgrads in ARG, Claire Raftery, Jason Byrne, Paul Conlon, for all their help. Finally, thank you to anyone else I barraged with questions along the way!

# CONTENTS PAGE

# CHAPTER 1: INTRODUCTION AND THEORY

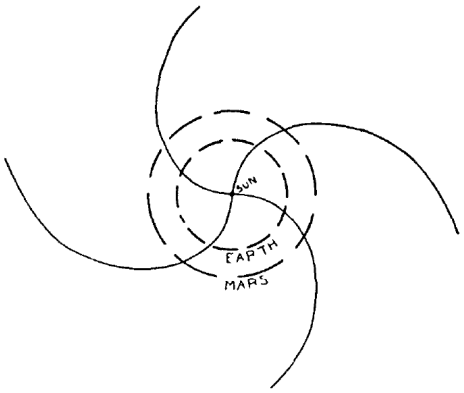


*Figure 1: Projection onto the Solar equatorial plane of the lines of force of any solar field which is carried to infinity by outward streaming gas with velocity $10^3$ km/s [Parker, 1958].*

The ionosphere is the part of the Earth's atmosphere that is ionised by solar UV and X-Ray radiation. It's structure is strongly influenced by the solar wind, which is in turn governed by the level of Solar activity. It is continually blasted by particles and energy from the Sun. The ionosphere reacts strongly to the intense x-ray and ultraviolet radiation released by the Sun during a solar flare or solar storm. These solar disturbances can be examined by monitoring changes to the Earth's ionosphere. The AWESOME (Atmospheric Weather Electromagnetic System for Observation Modelling and Education) monitor was designed by the Very Low Frequency Research Group at Stanford University, California, USA. It monitors changes in the ionosphere from radio waves being reflected off it. From the data obtained by the monitor it will be possible to observe daily changes in the ionosphere, solar events such as flares, and also Earth atmospherics, e.g. lightning strikes.

## 1.1 Solar Activity

### *1.1.1 The Photosphere and the Solar Wind*

The photosphere is the visible surface of the Sun. It is composed of convection cells called granules, and its radiation spectrum is similar to that of a blackbody[1] at 5777 K

[1] Blackbody: a thermodynamic system that radiates at its own equilibrium temperature[1]. One looks to the Stefan-Boltzmann Law, with the Stefan constant of $5.67 \times 10^{-8} Wm^{-2}K^{-4}$

[Lilensten & Bornarel 2006]. The photosphere is a primary site from which electromagnetic waves and the solar wind are emitted. The solar wind is closely related to the presence of a solar magnetic field. A convection of plasma creates a local magnetic field on the Sun, with local North and South poles. These poles are linked by field lines around which plasma travels. The magnetic field lines, carried by the plasma, stretch toward the outer region of the Sun into interplanetary space, but not actually leaving the Sun. Once it has left the Sun, the field is called interplanetary, and plasma becomes the solar wind. The solar wind, which blows at speeds of 300–800 km/s, corresponds to proton energies of 0.5–3 keV [Reames 2004].

The dynamic pressure $P_G = \frac{1}{2}\rho v^2$ of the solar wind dominates over the magnetic pressure $P_B=B^2/(8\pi)$ through most of the solar system, also called the heliosphere. The magnetic field is pulled into an Archimedean 'Parker' spiral pattern[2] [Parker 1958] by the combination of the outward motion and the Sun's rotation. In polar coordinates the Archimedean spiral can be represented by $r = a + b\theta$, where a and b are real numbers. Changing a will turn the spiral, while b controls the distance between successive turnings. However it has been suggested that the field must be somewhat more complicated than the simple picture [Giacalone & Jokipii 2001; Smith & Bieber 1991]. Research has suggested that deviation from the radial direction is greater than that for Parker's Spiral [Ajabshirizadeh & Filippov 2004].

As the solar wind expands, its density decreases as the inverse of the square of its distance from the Sun. Eventually the solar wind's strength is no longer great enough to push back the interstellar medium. This point is known as the heliopause, and is generally considered to be the outer boundary of the solar system. In 2003, the spacecraft Voyager I (launched with Voyager II by NASA in 1977) reached the so-called termination shock of the solar wind, at 85Au from the Sun [Fisk 2003]. There was some disagreement to this [See McDonald et al. 2003; Krimgis et al. 2003]. In 2006 it was announced that Voyager should reach the boundary within a year, leading

[2] Archimedes Spiral: The locus of points corresponding to the locations over time of a point moving away from a fixed point with a constant speed along a line which rotates with constant angular velocity.

[2a] http://www.cnn.com/2006/TECH/space/05/23/voyager.2/index.html

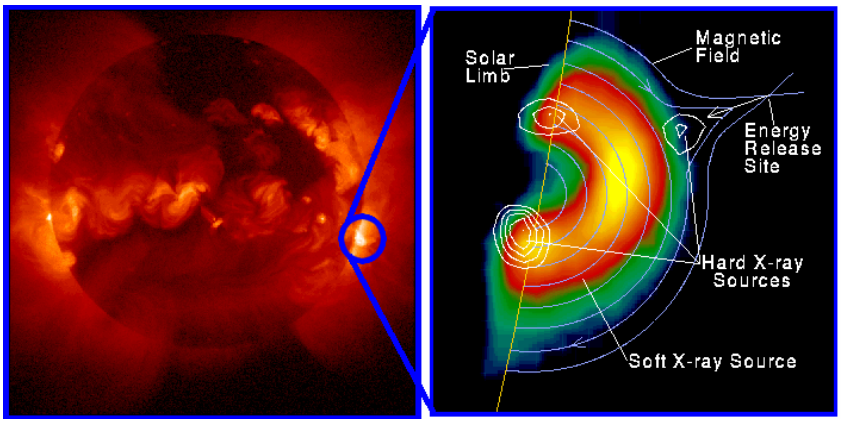


*Figure 2: Yohkoh image of a solar flare, combined image in soft x-rays(left) and soft x-rays with hard x-ray contours (right) [Yohkoh 1992].*

---

to suggestions that the edge of the shock is about one billion miles closer to the sun in the southern region of the solar system than in the north.[2a]

*1.1.2 Sunspots and solar flares*

Sunspots are dark zones on the Sun's surface, mainly located at latitudes between 40°N and 40°S [Lilensten & Bornarel 2006]. They appear darker since their temperature is lower than the rest of the surface, ~4000 K. The magnetic field inside the spots is from 100 to 5000 times more intense than the surrounding field. When the Sun's activity is quiet there are few or no, but in an active period there is a high number of sunspots.

How are they formed? One must look to the surface magnetic field of the sun. This shows up as field lines that are perpendicular to the surface but can be found both above and below the photosphere. However matter revolves more slowly at high latitudes than at lower ones, and more quickly near the interior of the surface. Under the effect of these rotations, magnetic field lines are distorted and become more complex in shape. When the field lines become very dense a pore [Phillips 1992] forms on the surface, which gives rise to local intense magnetic field tubes that are perpendicular to the surface. Here the field lines suppress cross-field heat conduction; the gas cools down, and a spot is formed.

The magnetic 'Hale' cycle (discovered in 1925) is a 22 year one[3]. The magnetic polarities of the sunspots reverse from one 11year sunspot Schwabe [Scwabe 1843] cycle to the next. The behaviour of the entire solar magnetic field is governed by this inversion.

The spots are decayed and fragmented by the motion of matter of supergranulations[4]. Sometimes filaments can form above the spot, which is a long structure that seems darker because it rises from the lower colder layers to hotter ones. Active region prominences are so-called if the prominence occurs on the side of the Sun facing us. Sometimes these can give rise to solar flares, when the energy trapped in the sunspot B-fields is suddenly released.

*1.1.3 Coronal Holes*

At a transition region of the solar atmosphere between ~3000 km and few tens of km, there is a sudden quick temperature increase from ~ $10^3$ K to $10^4$ K, and it can reach a few million Kelvin very quickly. Above this region of intense heat one can find coronal holes, which are mobile low density structures that are cooler than the corona and cover up to 1/3 of the Sun's surface [Lilensten & Bornarel 2006]. At the poles, their magnetic field opens widely towards space, and this provides an exit of sorts for the solar wind. Large plumes of matter break free from the holes, and are far bigger than spicules[5]. The solar 'fast' wind from the plumes blows almost twice as fast as the slower wind. Research from Arge et al. (2003) has delved into the origins of the solar wind, however it's origin is still unclear [Marsch 2005].

*1.1.4 Coronal Mass Ejections*

These can be described as observable changes in the coronal structure, and pre-empt an expulsion of plasma and magnetic field from the corona toward interplanetary space. They scale much greater than solar flares, with masses $\geq 10^{16}$g, and kinetic energies $\geq 10^{25}$J [Antiochos et al. 1998]; and affect more than 1/3 of the corona, at altitudes of several solar radii [Lilensten & Bornarel 2006].

---

[3] One can see this in Hale's polarity Law, which states that the polarity of the foremost spots in one of the hemispheres is the opposite of that in the other hemisphere.

[4] Supergranulations: particular pattern on the Sun surface. It was discovered in the 1950's by A.B.Hart on Doppler velocity measurements showing horizontal flows on the photosphere.

[5] Spicule: a dynamic jet ~ 500km diameter on the Sun. It moves upwards at ~ 20 km/s from the photosphere. Discovered in 1877 by Father Angelo Secchi of the Vatican Observatory in Rome[De Pontieu et al, 2004]

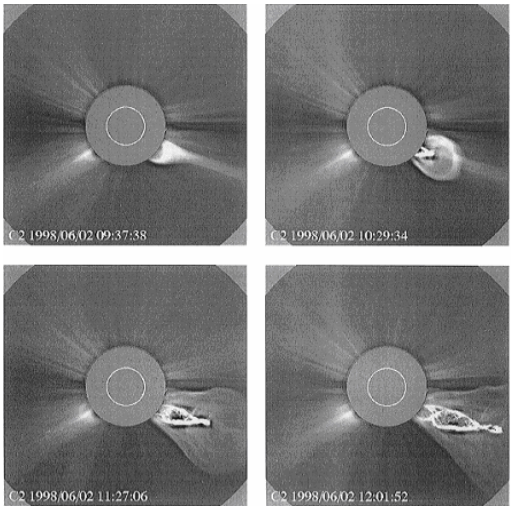


*Figure 3: Evolution of a "three-part" CME observed by the SOHO LASCO C2 and C3 coronagraphs on 2 June 1998 [Webb 2000; Plunkett et al. 2000].*

. When an eruption occurs, the lost matter leads to a local depletion and a temporary coronal hole. When the hole is filled (immediately), displacements of matter in the form of 'Moreton waves' occur, which spread out over the whole corona. Observations have determined expulsion speeds from 20 to 2600km/s [Manchester et al, 2005].

CMEs can exhibit a variety of forms, some having a 'three-part' structure and others having more complex structure with interiors filled with bright emitting material [Webb 2000; Howard et al. 1997].

### 1.2 The Earth's Atmosphere

The Earth's atmosphere can be said to be split up into a number of layers. The troposphere is the lowest part of the atmosphere. Mainly molecular oxygen is found here, and all weather is confined here. Pressure and density decrease in function of altitude following the exponential barometric law[6][ Lilensten & Bornarel 2006].

The stratosphere is mainly responsible for absorbing the ultraviolet radiation from the Sun. Within the stratosphere, solar radiation breaks up molecular oxygen $O_2$ into individual oxygen atoms. Each of these atoms may combine with an $O_2$ molecule

[6] Barometric Law: pressure P(z) as a function of height z from the surface of a planet's atmosphere varies as $P(z) = P_o e^{-mgz/(kT)}$; m is defined as the molecular mass, g the gravitational acceleration, k is Boltzmann's constant, and T is the temperature.

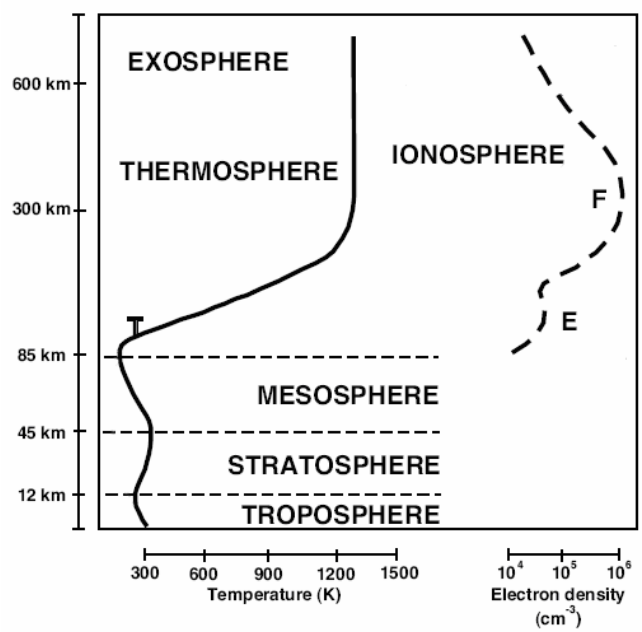


*Figure 4: Earth's atmosphere varies in density, composition and temperature as the altitude increases above the surface.*

---

to form ozone, $O_3$[Welch].

In the mesosphere, the temperatures falls as low as 180K with increasing altitude[Phillips 1995]. This is due to the concentration of ozone decreasing, so its dissociation is no longer a source of warming up[Lilensten & Bornarel 2006].

These lower layers are known as the homosphere, up to about 85km. The molecules and atoms mingle, producing a homogenous gas. The gas becomes increasingly rarefied at higher altitudes. Above the homosphere, space begins at the heterosphere, around 80km. The gas is so thin that free electrons can exist for short intervals before they are captured by a nearby positive ion. Beyond the Atmosphere, the exosphere starts at the top of the ionosphere and continues until it merges with interplanetary gases, or space. In this region of the atmosphere, Hydrogen and Helium are the prime components and are only present at extremely low densities [Phillips 1995].

The mesopause separates the mesosphere from the ionosphere**,** which is the subject of study for this report. It extends to 600 km, and the temperature increases with increasing altitude due to the Sun's energy. Temperatures can reach as high as 2000 K. The ionopause occurs at a height where the pressure due to the solar wind equals the pressure of the planetary atmosphere, i.e., *Psw = Ppa.*

*1.2.1 The Ionosphere*

Solar radiation strikes the atmosphere with a power density of 1370 $W/m^2$, the 'solar constant,' found from $L = A\sigma T^4$. This intense level of radiation is spread over a broad spectrum ranging from radio frequencies to IR, and visible light to X-rays. Solar radiation at UV and shorter is considered to be ionising. This is because photons of energy at these particular frequencies are able to dislodge an electron from a neutral gas atom or molecule during a collision.

So the solar radiation is incident on the gas atom, and part of this radiation is absorbed by the atom. A free electron and positively charged ion are produced. Cosmic rays and solar wind particles also play a role in this process but their effect is minor compared with that due to the sun's electromagnetic radiation [Kelley & Heelis 1989].

As the altitude decreases from high up in the Earth's atmosphere the ionisation process increases because more gas atoms are present. However, recombination then also begins to occur. Here if a free electron moves near enough to a positive ion, it is captured by it. So at lower altitudes where the gas density is greater, more and more recombination takes place. The point of balance between these two processes determines the degree of "ionisation" present at any given time [Kelley & Heelis 1989].

As the altitude decreases further, the numbers of atoms and molecules of gas increase further, so there is more opportunity for absorption of energy from a photon of UV solar radiation. At lower altitudes the intensity of this radiation is smaller because some of it was absorbed at the higher levels. Thus a point is reached where lower radiation, greater gas density and greater recombination rates balance out. The ionisation rate then begins to decrease with decreasing altitude. This leads to the formation of ionisation peaks or layers [Kelley & Heelis 1989]. These are called Heaviside layers.

As seen in figure 5, the composition of the atmosphere changes with height, so the ion production rate also changes and this leads to the formation of these several distinct ionisation peaks, the D, E, F1, and F2 layers.

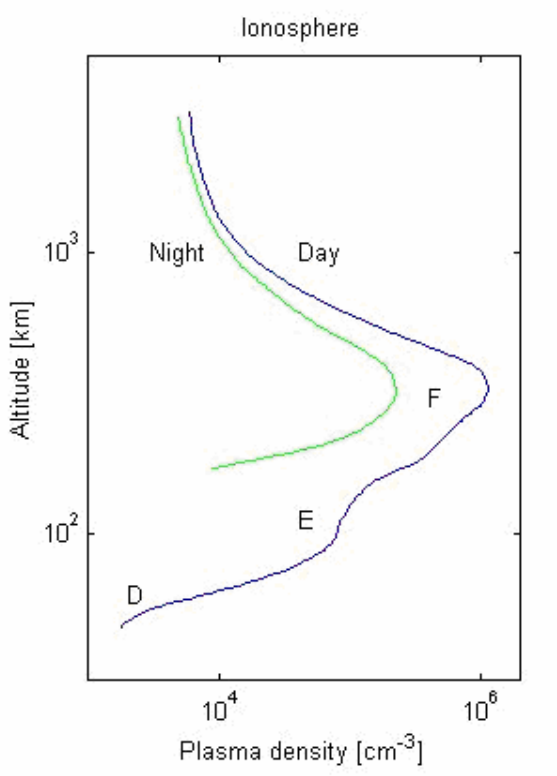


*Figure 5: Variation of plasma density vs. altitude for daytime and nighttime*[7]

---

*1.2.2 The Ionospheric Layers*

D Layer

The D layer is the innermost layer, 50 - 90 km above the surface of the Earth. Negative ions prevail here, and electrons are produced by the ionisation of oxygen and nitrogen by soft X-rays, of wavelength less than 1nm [Phillips 1992], which are strongly enhanced during period of solar activity, e.g. solar flares. Ionisation is also due to Lyman series-alpha hydrogen radiation at a wavelength of 121.5 nm, ionising a nitric oxide molecule, NO [Phillips 1992]. Cosmic rays from outside the solar system can also produce significant ionisation in the D layer.

E Layer

The E layer is the middle layer, 90 - 120 km above the surface of the Earth. Positive molecular ions are in the majority, mainly $O_2^+$ and $NO^+$. Ionisation is due to soft X-ray (1-10 nm) and far ultraviolet (UV) solar radiation ionisation of molecular oxygen [Phillips 1992].

[7] Oulu Space Physics Textbook, http://www.oulu.fi/~spaceweb/textbook/

F Layer

The F layer, also known as the Appleton[8] layer, is 120 km to 400 km above the surface of the Earth. Here extreme UV (10-100 nm) solar radiation ionises atomic oxygen, O. The F layer combines into one layer at night, and in the presence of sunlight (during daytime), it divides into two layers, the F1 and F2.

- F1: transition between the molecular ions (primarily $O^+$) and the positive atomic ions (mainly $O^+$).
- F2: $O^+$ is the principal ionic type, characterised by the transition between photochemical mechanisms (lower part) and diffusion mechanisms (upper part).

[Lilensten & Bornarel 2006]

*1.2.3 The Geomagnetic field and Magnetosphere*

Earth's magnetic field (and the surface magnetic field) is approximately a magnetic dipole, with one pole near the North Pole and the other near the geographic South Pole. An imaginary line joining the magnetic poles would be inclined by approximately 11.3° [NOAA 2005] from the planet's axis of rotation. The cause of the field is probably explained by dynamo theory[9] [See Schatten 2003].

The iron-nickel core of the Earth acts as a giant magnet, comparable to a dipole bar magnet, but this similarity is superficial. The magnetic field of a bar magnet, or any other type of permanent magnet, is created by the co-ordinated spins of electrons and nuclei within iron atoms. The Earth's core, however, is hotter than 1043 K, the Curie point temperature at which the orientations of spins within iron become randomised [Roach 2004]. This randomisation causes the substance to lose its magnetic field. Therefore the Earth's magnetic field is caused not by magnetised iron deposits, but mostly by electric currents in the liquid external core.

The magnetic field extends as the magnetosphere, above 600km, for several thousand km. Above here, particle concentration becomes so low that their behaviour is no longer a function of collisions but is a but is a consequence of the configuration of the magnetic field.

[8] Appleton layer, the highest region of the ionosphere, named after Sir Edward Appleton, who proved the existence of the Heaviside layer.

[9] Dynamo Theory: describes the process through which motion of a conductive body in the presence of a magnetic field acts to regenerate that magnetic field.

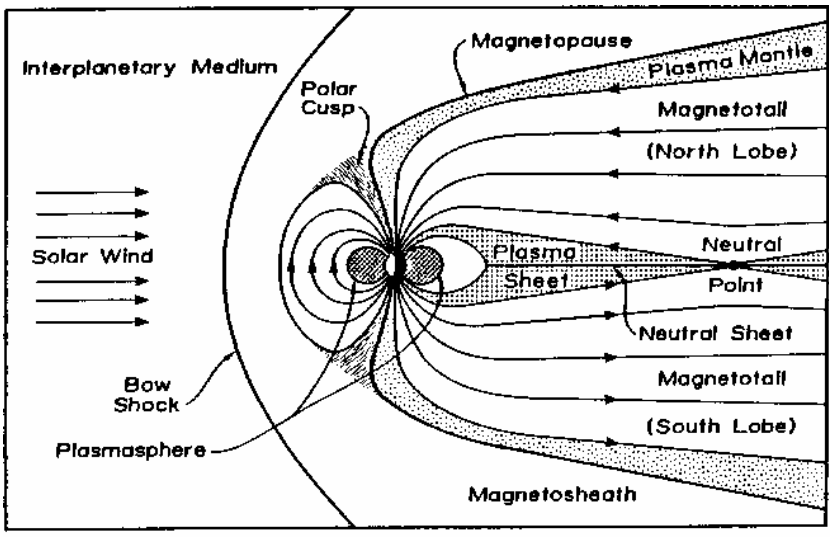


*Figure 6: An illustration showing the regions of the magnetosphere [Russell, UCLA].*

---

*1.2.4 Regions of the Magnetosphere*

The solar wind particles flowing directly from the Sun toward the Earth must go around the magnetosphere obstacle, but due to their high speed, their direction is changed abruptly in the bow shock region, lying just outside magnetic field facing the Sun.

The particles reduce speed and change their motion when passing through this region. Most of the shocked solar wind particles are deflected around the magnetosphere through an area called the magnetosheath. This region effectively shields the Earth from most of the direct solar wind because charged particles do not readily travel across a magnetic field but are deflected at angles to the magnetic field.

Some of the plasma from the solar wind can, however, travel along the magnetic field lines of the Earth, leaking through the Earth's magnetic screen. The polar cusps are two funnel-shaped regions, which lie between the sunward magnetic field and the tailward magnetic field [Green 2004]. When the solar wind enters the polar cusp, it follows the magnetic field lines toward Earth. Through the polar cusps, high-speed charged particles from the solar wind bombard our upper atmosphere. The cusps are known to be weak-field regions.

In contrast to the sunward magnetosphere, compressed and confined by the solar wind, the tailward is stretched out into a long "magnetotail"[See Galperin 1995]. It is a dynamic part of the magnetosphere, and ions and electrons are often energised there. It is also the main source for polar auroras.

The volume of the tail is mainly taken up with the two tail lobes[11]. These lobes lie adjacent to the plasma sheet, and the very thin boundary between the plasma sheet and the tail lobes is called the plasma sheet boundary layer.

In the upper (northern) half of the plasma sheet, the magnetic field is directed toward Earth; in the lower (southern) half, the field is directed away from the Earth. As long as the impact of the solar wind on the magnetosphere remains fairly steady, the plasma sheet exists in equilibrium. When the plasma sheet balance is disturbed, its dimensions are altered radically, with consequences throughout the magnetosphere.

High-energy electrons and protons are trapped by the earth's dipole magnetic field in the Van Allen Radiation Belt. It consists of two distinct doughnut-shaped regions encircling the earth, the first being the inner belt, at about $1.5R_e$. The most penetrating particles here are hard protons with energies of several tens of MeV. The outer region is found at about $3.5R_e$. Here the most penetrating particles are electrons, with energies up to several MeV [Okada & Iwai 1988].

Each of the regions of the magnetosphere discussed above have unique magnetic field topologies, particle populations, and electron and ion flow velocities. The solar wind is responsible for the overall shape of the magnetosphere, and fluctuations in its speed, density, direction, and entrained magnetic field strongly affect Earth's local space environment. This leads to what can be called space weather.

### *1.2.5 VLF Radio Wave Propagation*

Radio propagation is used to explain how radio waves behave when they are transmitted, or are propagated from one point on the Earth to another. VLF waves are in the region 3 - 30 kHz , and are guided between the earth and the ionosphere.

In "free space", all electromagnetic waves (radio, X-rays, visual, etc.) obey the inverse-square law. This states that an electromagnetic wave's strength is proportional to $1/(r^2)$, where r is the distance from the source. So, for example, if you double the distance from a transmitter, the strength is reduced to a quarter, and so on [Forbes et al. 2006].

There are numerous ways of propagation- ground wave, line-of-sight [Boithais & Lucien 1987]. The one of importance to this project is skywave propagation, which

[11] http://www-spof.gsfc.nasa.gov/Education/wtail.html

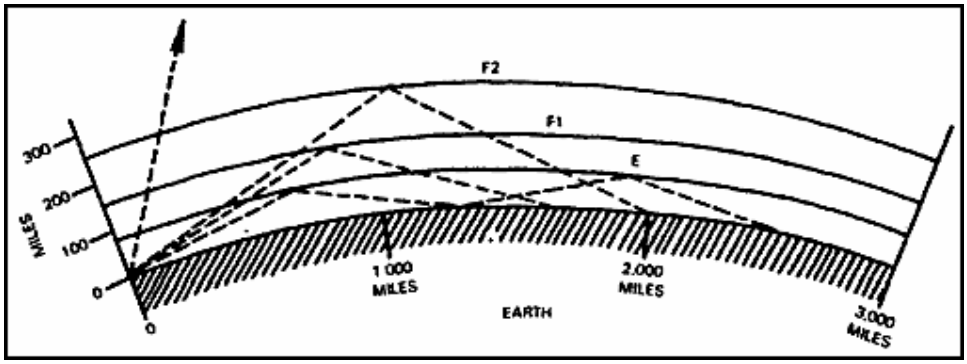


*Figure 7: Relating reflected waves to distances along earth's surface [AIPD].*

---

is any of the modes that rely on refraction of radio waves in the ionosphere, made up of its various ionised layers. The sun directly affects these layers on a daily cycle, and the 11-year cycle determines the utility of these modes.

Here, the radio waves are refracted back to the Earth's surface by the ionosphere. When the wave reaches the ionosphere, the wave's electric field forces the electrons in the ionosphere into oscillation[12] at the same frequency as the radio wave. Some of the energy of the radio wave is given up to this mechanical oscillation. The oscillating electron will then either be lost to recombination or will re-radiate the original wave energy back downward again. Total reflection can occur when the collision frequency of the ionosphere is less than the radio frequency, and if the electron density in the ionosphere is great enough [Boithais & Lucien 1987].

Depending on the transmitting antenna, some signals may reach the ionosphere at a steep angle (vertical incidence) and be reflected almost straight down. Alternately the antenna may aim the signal at the horizon; the signal reaches the ionosphere at a shallow angle, and returns to earth at a great distance.

Under some conditions, the Earth's surface may reflect the incoming wave back toward the ionosphere again. As a result, the wave may bounce between the earth and ionosphere several times, known as skip propagation. Signals of only a few watts can sometimes be received thousands of miles away as a result.[13]

Note that the condition of the ionosphere is constantly changing due to interaction with incoming radiation (solar activity). When waves bounce off an irregular surface, they may fade in and out and have a 'phasing' character.[15]

---

[12] Electrons accelerated in solar flares to energies of some keV are streaming away from the Sun and excite plasma oscillations locally. The plasma oscillation frequency has its origins in $m\ddot{x} = -eE$

[13] http://en.wikipedia.org/wiki/Skywave

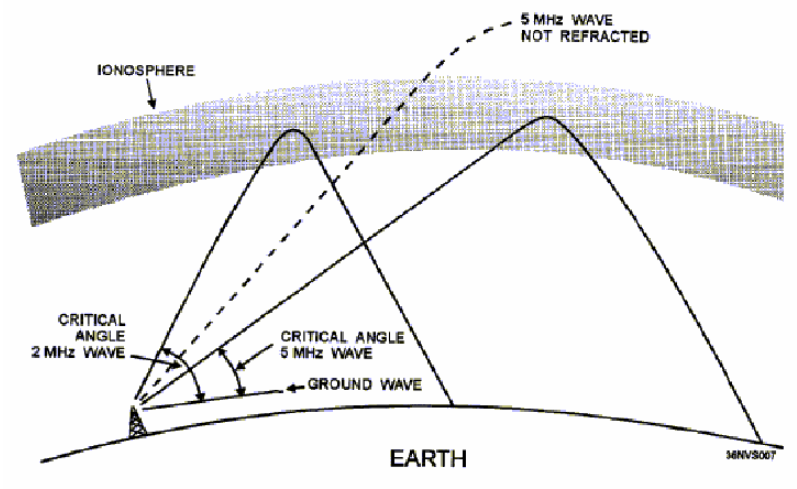


*Figure 8: The critical angle for radio waves depends on the layer density and the wavelength of the signal [US Navy].*

---

Some important Frequencies:

- The critical frequency is the limiting frequency at or below which a radio wave is reflected by an ionospheric layer at vertical incidence. The highly stratified layers of the ionosphere refract the VLF waves until the angle of incidence of the wave reaches the critical frequency. Any wave, at a given frequency, that leaves an antenna at an incidence angle greater than the critical angle will be lost into space.

$$f_{critical} = 9x10^{-3}\sqrt{N}$$

where N = electron density per $cm^3$ and $f_{critical}$ is in MHz.

The existence of the critical frequency is the result of electron limitation, i.e., the inadequacy of the existing number of free electrons to support reflection at higher frequencies.

- The higher the frequency of a radio wave, the lower the rate of refraction by the ionosphere. Therefore, for a given angle of incidence and time of day, there is a maximum frequency that can be used for communications between two given locations. The Maximum Usable Frequency (MUF) is defined as the upper frequency limit that can be used for transmission between two points at a specified time:

$$f_{muf} = \frac{f_{critical}}{\sin\alpha}$$

where α = angle of attack, the angle of the wave relative to the horizon, and sin is the sine function.

Waves at frequencies above the MUF are normally refracted so slowly that they return to earth beyond the desired location or pass on through the ionosphere and are lost.

- The cut-off frequency is the frequency below which a radio wave fails to penetrate a layer of the ionosphere at the incidence angle required for transmission between two specified points by reflection from the layer. As the frequency of a radio wave is lowered, the rate of refraction increases. So a wave whose frequency is below the established cut-off frequency is refracted back to earth at a shorter distance than desired. For a rectangular waveguide,

$$F_c = \frac{c}{2h},$$

where c = speed of light, and h = height (e.g. reflection height of the ionosphere) [Thierry 2003].

# CHAPTER 2: EXPERIMENTAL METHOD

*Figure 9: 5 way cross connecting base pipes and vertical pipe.*

*Figure 10: Antenna wires resting on detractable socket to allow for easy dismantling.*

## 2.1 AWESOME Antenna

A list of equipment used for the construction of the antenna can be found in Appendix 1. Following is a description of the set-up procedure:

### *2.1.1 Apparatus set-up*

The GPS antenna was secured to a wooden mast using cable ties, and fixed to the roof, in a place where it had as much sky coverage as possible (at least 3 satellites were needed for a GPS lock). It was then connected to the line receiver via the N-type cable.

The line receiver was plugged into a power outlet. It was then connected to the computer via two connections; the first being a cable going from the PC ADC slot on

*Figure 11: Complete set-up of antenna on the roof of the SNIAMs building, TCD.*

---

the line receiver to the corresponding PC card slot on the back of the PC, the second a serial cable going from the line receiver to a serial port on the PC.
The line receiver was connected to the preamplifier with the 14 pin cable.

*2.1.2 Construction of Antenna Mount*

- An isosceles triangle antenna was to be constructed, with the antenna making a 45° angle at both corners to the ground, and a 90° angle at the top (mast).
- Five lengths of the 1" PVC piping were sawed to equal lengths of 1.3m.
- Grooves were sawed into the tops of the pipes so that the looped antenna wire could feed through them. A hacksaw was used to cut two equal depth parallel slits, and pliers used to snap off the inner section. The same was done to the exact opposite side of the pipe. The result was filed down to ensure a smooth surface for the wire to rest on.
- A 5way cross piece was constructed from a 3 way 1" T-piece and a 1" socket in the Mechanical Workshop in the School of Physics, TCD (see figure 9). A section was cut out of the T-piece through which the socket would slide. So the T piece would act as 2 sides of the base section and the vertical part, and the socket the other two sides of the base section. The parts were cemented together to ensure stability.
- It was necessary to be able to take the mount apart for ease of transport. So a device was constructed (see Figure10) in order to be able to detract the length of the vertical pipe and remove the looped wire. A hole was drilled

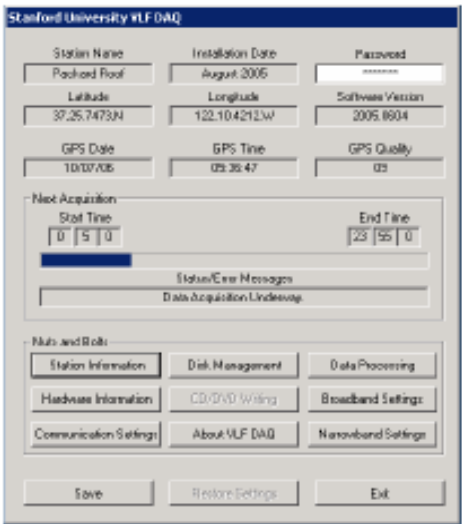


*Figure 12: Image of the VLF_DAQ Console*

---

through a 1" socket into the top of the pipe, and a bolt slid through and held into place with a washer.

- The 1.3m length pipes were connected together using the five-way cross piece, and the wire looped across it (See Figure11).

*2.1.3 Combining components*

Once the looped antenna wire was placed on the mount, the antenna was oriented in such a fashion that the NS antenna was in the NS plane, and EW loop in EW plane. The antenna was then connected to the preamplifier. This was connected in such a way that the polarity was configured as so: Standing to the North of the EW antenna, looking south, following the antenna loop from + to –, the antenna loop should be clockwise. Standing east of the NS antenna looking west, + to – should go clockwise.

*2.1.4 Software*

The NI6034E card was installed into the computer's PCI slot, and the 'Traditional Ni-DAQ 7' software accompanying it was installed. The Stanford VLF_DAQ software was then installed to the C:\. The VLF_DAQ console was opened and the settings that suited this project best were configured. See Appendix 2 for full details of the settings.

The settings were set for a number of transmitters at the following frequencies:

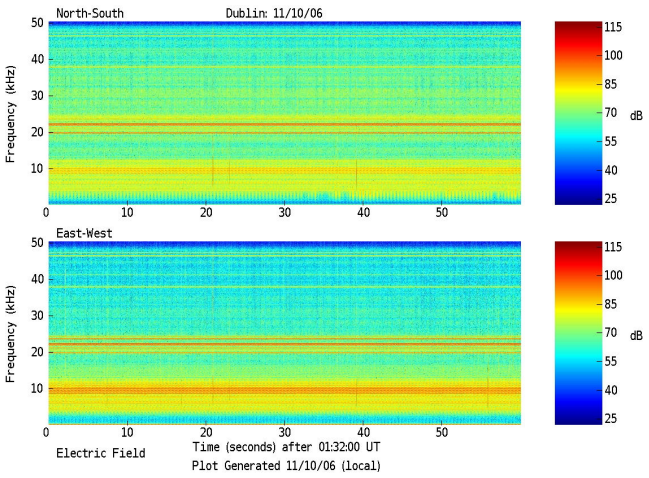


*Figure 13: Sample broadband spectrum, on October 11th 2006. The horizontal lines represent the transmitter frequencies.*

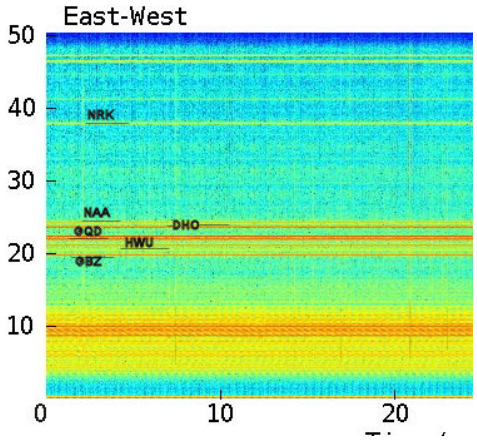


*Figure 14: Zoomed in image of Figure 10, with transmitter frequencies marked.*

---

GQD: 22100Hz (Anthorn, UK)

HWU: 20900Hz (Rosnay, France)

DHO: 23400Hz (Rhauderfehn, Germany)

NRK: 37500Hz (Grindavik, Iceland)

NAA: 2400Hz (Cutler, Maine, USA)

The best frequencies could be found from examining a sample spectrogram. In figures 13 and 14 the horizontal lines correspond to the transmitters at various frequencies.

Once the pre-amplifier was connected to the line receiver, and everything set up as above, it was now possible to begin collecting data.

### *2.1.5 Data Acquisition and Analysis*

Once the VLF_DAQ software had been installed and configured, all that had to be done to start the acquisition of data was to run the VLF_DAQ program. Once a GPS lock had been obtained, the data began to be collected. It would save into a data folder as two types of .mat files: narrowband and broadband files.

The broadband recording saved the waveform received from the antenna exactly as it was received, at the full 100 kHz sampling rate. It included all information between the cut-off frequencies of 330 Hz and 47 kHz. It saved at a rate of 1.5 GB per hour, and so, due to storage limitations, it was only saved in 10minute snippets, capturing an example at 3am at night and 3pm in the afternoon. It saved in the following format:

XXYYMMDDHHMMSS_ACC.mat

*Where, XX= Station ID; YY= Year; MM = Month; DD = Day; HH = Hour; MM = Minute; SS = Second; A = zero-based index of the ADC card used; CC = zero-based index of the software channel number used.*

A spectrogram .jpg file also saved to the harddrive, one per minute. Once permission to ftp was obtained from IS Services in TCD, the VLF_DAQ program was configured to ftp these spectrogram images to the Very Low Frequency Group at Stanford University continuously so that it could be shown live on the Stanford webpage:

http://www-star.stanford.edu/~vlf/hardware/fieldsites/dublin/dublinlive.html

The narrowband recording took the amplitude and phase of a single narrow frequency range, corresponding to the frequency of a VLF transmitter. The data saved in a hi-resolution (50 Hz) and a low-res (1 Hz). This data saved at a rate of 1 MB per hour, and so saved to the harddrive continuously, except during the hours of 12pm-2pm, when the data files would be ftped to Stanford for their records. The format of this file is:

XXYYMMDDHHMMSSZZZ_ACCT.mat

*Where, XX, YY, MM, DD, HH, MM, SS, CC, A are as for the broadband data, and*

*ZZZ = Transmitter callsign; T = Amplitude/Phase or Low/High resolution. Here, A = Lo resolution amplitude (1Hz sampling rate), B = low res phase, C = high res amplitude, D = high res phase.*

These data files could then be examined using Matlab. The data list as it appears in Matlab can be found in Appendix 2.

Using specifically designed commands from Stanford, plots of the data could then be plotted using Matlab. The vlf_spec command was used to view the broadband files, which gave three different plots (see results). The fft command was included in the vlf_spec command, however it could also be done manually, see Appendix 3(a) for details.

The narrowqplot command was used to view narrowband data, displaying amplitude and phase (see results). If the narrowband files did not save in one file for a 24hour period, several data files could be plotted together using the plot command, detailed in Appendix 3(b). Origin and Excel were also used at times to plot some of the data.

# CHAPTER 3: RESULTS

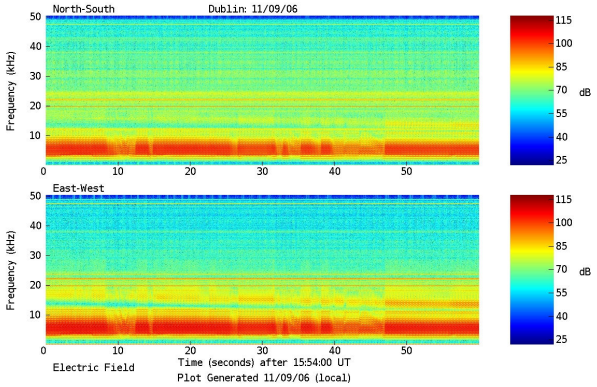


*Figure 15(a)*

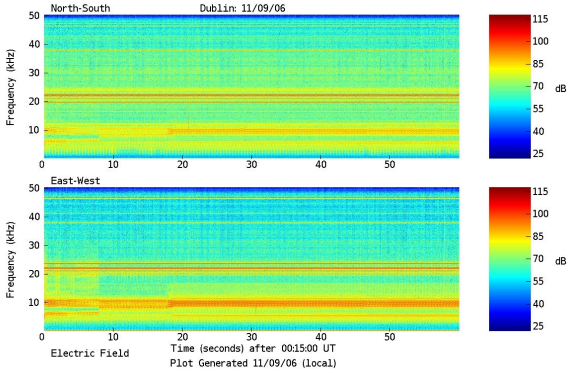


*Figure 15(b*

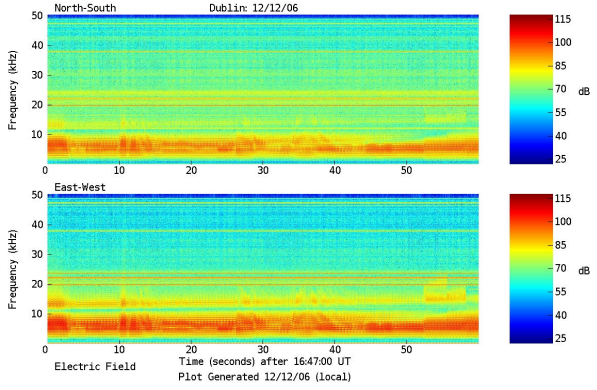


*Figure 15(c)*

*Figure 15 shows varying noise in spectra from different times of the day: It shows N-S and E-W Broadband spectrum at 15(a) 15:54 UT on November 9th 2006; (b) at from 00:15UT on November 9th 2006; (c) at 16:47UT on December 12th 2006.*

### 3.1 Sferics

The broadband data produced continuous spectra saved as one-minute long jpg files, such as in Figure 15 (a). In this image, the horizontal transmitter lines can be seen from above about 20 kHz (as in Figure14). However in this spectrum, as well as the majority of the others obtained, there is a large amount of noise. This is the 'red' at the bottom of the spectrum, from about 10 kHz and below. The noise seemed to be at it's greatest during the day, and tended to either decrease or disappear completely at night-time, as in Figure 15 (b).

The noise also decreased significantly during the weekend compare to during the week, as one can see in Figure 15 (c).

Hence, the noise was probably background noise from equipment in one of the surrounding buildings in TCD. It did not affect the data from the transmitters, as the frequency region is too low for that; however it did affect the accuracy of calculations relating to sferics, as the cut-off frequencies were in the 2 kHz range. The noise could be somewhat removed using Matlab (see 'Sferics' Section), however its impact on accuracy was still significant.

Once the broadband files were loaded into Matlab, it was possible to plot a number of graphs for both N/S and E/W antennas. The timescale could be altered, as well as the offset from the start of the file. Say, for example, there was a file with 60 seconds worth of data from 3am on the November 16$^{th}$ 2006. If data from 03:00:00 - 03:00:10 a.m. was to be plotted, the timescale would be set to 10 seconds, and the offset equal zero.

Figures 16 (a), (b), and (c) show typical broadband plots of what was obtained using Matlab. A spectra and magnetic field plot would be obtained as in Figures 16 (a) and 16 (b). A full fft could also be made on the spectrum, producing a plot like in Figure 16 (c).

Examining the graph in Figure 16 (c), one can see the correlation between the small peaks in the region 20-25 kHz and the horizontal lines in Figure 16 (a), showing the transmitter frequencies.

Looking again at Figure 16 (a), a vertical line peaking about 10 kHz, at 03:00:02 UT, represents a lighting strike. This can be zoomed in for closer inspection, as in Figure 17.

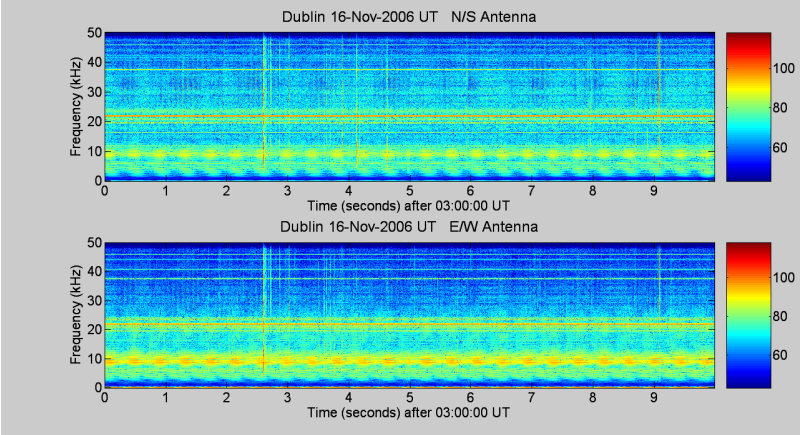


*Figure 16(a)*

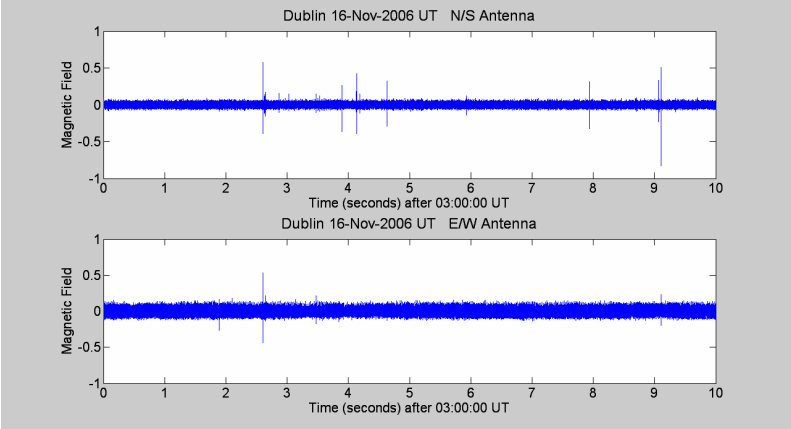


*Figure 16(b)*

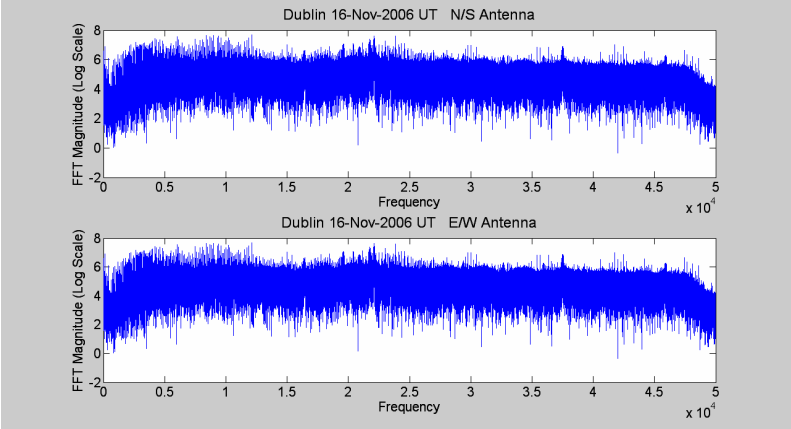


*Figure16(c)*

*Figure 16 shows the results from using the 'vlf_spec' command in Matlab on a data file from 3am on November 16th 2006. 16(a) is a broadband spectrum; 16(b) a magnetic field plot; 16(c) an fft plot*

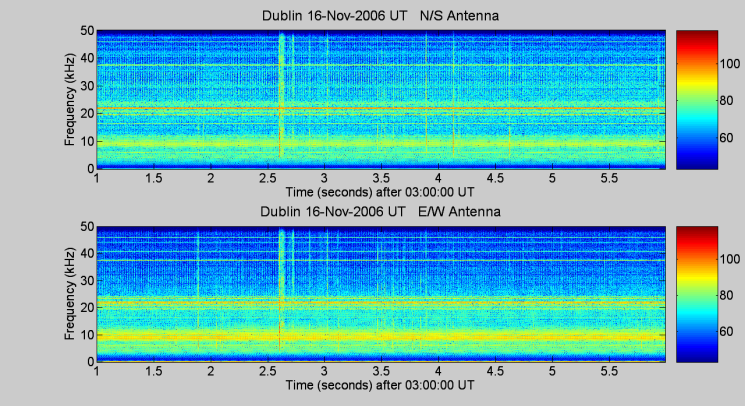


*Figure 17: Zoomed-in spectra from N/S and E/W antennas at 3am UT on November 16th 2006.*

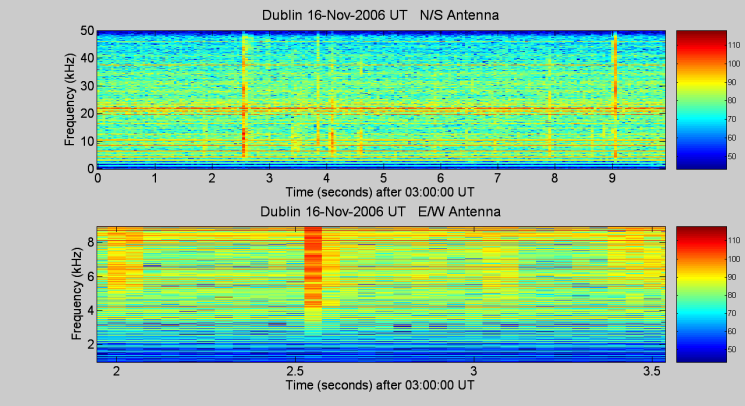


*Figure 1817: Zoomed-in image of figure 25, with fft window altered to $10^3$.*

---

*3.1.1 Reflection Height and Electron Density*

The next step was to calculate the cut-off frequency, and from this determine the reflection height of the ionosphere at the event, and the electron density at that height.

As mentioned earlier, due to the noise, it was rather difficult to determine the exact cut-off frequency. Even on this graph at 3am there was some noise. Therefore, to try to remove some of it, the code for the vlf_spec command was altered in order to create longer fft windows. The default value of 1024 was changed to something larger, for example, $10^3$, until some sort of cut-off point could be estimated. Time resolution was lost, but it was necessary for an accurate as possible value.

For the spectrum in Figure 17, once the value was changed to $10^3$, and the cut-off region zoomed in, the spectrum looked like Figure 18.

Even with changing the fft window, one does not see a proper cut-off 'curve' as in Figure 19 [Thiery 2003]. In Figure 20, the characteristic curved sferic cut-off can also be seen, in an image received from the Wilcox AWESOME monitor receiver.

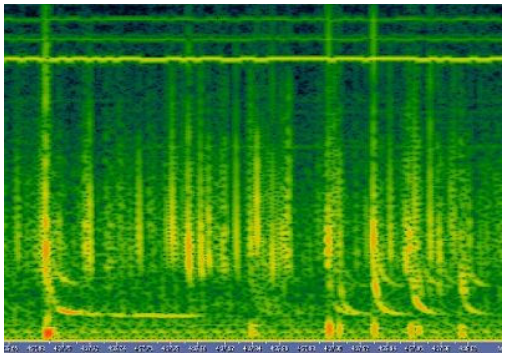

*Figure 19: Image showing a sudden spheric stop at around 3 Khz [Thierry 2003].*

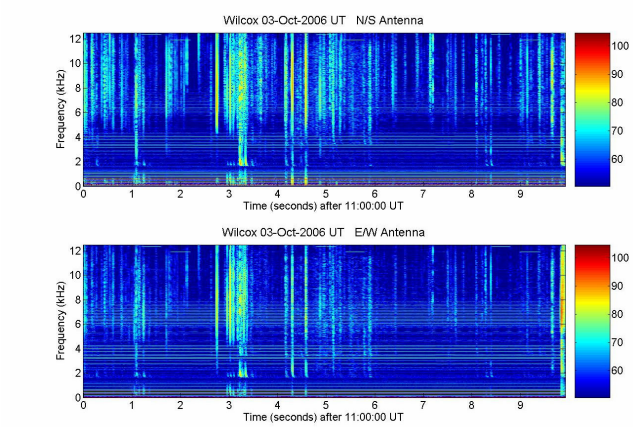


*Figure 2018: Broadband spectrum from Wilcox Receiver, California, at 11:00UT on October 3rd 2006.*

---

Since the curve could not be seen at the bottom of the spectra from the Dublin antenna, the cut-off frequency was estimated, and a large error of ±0.5 kHz was included. For the spectrum on the 16th, the cut-off was taken to be (2.3 ± 0.5) kHz.

For a rectangular waveguide, the cut-off frequency Fc is given by

$$F_c = \frac{c}{2h}$$

Where c = speed of light = 3 x $10^8$m/s, and h = vertical height of the waveguide.

Therefore, the reflection height of the ionosphere can be calculated from

$$h = \frac{c}{2f_c} \quad \text{[Thierry 2003]}$$

Also, the electron density can be calculated from $f_c$ using

$$n_e(cm^{-3}) = 1.241x10^{-8} f_c f_h$$

Where $f_h$ = cyclotron freq depending on your latitude [Ohya et al 2003].

Using the International Geomagnetic Reference Field model[14], and taking Dublin's latitude to be 53°21'N, $f_h$ = 13.716 MHz

Looking at various lightning strikes that were picked up by the monitor, the reflection height of the ionosphere and the electron density at that height could be calculated for various times (for figures see Appendix 4). Table1 summarises the results.

| Date (Nov/Dec '06) | Time (UT) | Night or Day | $F_c$ (kHz) | ΔFc (kHz) | h (km) | Δh(km) | $N_e(cm^{-3})$ | $\Delta n_e(cm^{-3})$ |
|---|---|---|---|---|---|---|---|---|
| 16 | 03:00:02 | Night | 1.8 | 0.4 | 83.2757 | 18.5057 | 306.3880 | 68.0862 |
| 19 | 03:00:06 | Night | 2.2 | 0.4 | 68.1346 | 12.3881 | 374.4742 | 68.0862 |
| 27 | 15:00:05 | Day | 2.1 | 0.4 | 71.3792 | 13.5960 | 357.4527 | 68.0862 |
| 28 | 16:13:10 | Day | 2.5 | 0.4 | 59.9585 | 9.5934 | 425.5389 | 68.0862 |
| 29 | 07:08 | Night | 1.7 | 0.4 | 88.1743 | 20.7469 | 289.3665 | 68.0862 |
| 29 | 07:29:37 | Night | 1.75 | 0.4 | 85.6550 | 19.5783 | 297.8772 | 68.0862 |
| 29 | 07:51:24 | Day | 2.3 | 0.4 | 65.1723 | 11.3343 | 391.4958 | 68.0862 |
| 2 | 10:01:09 | Day | 1.8 | 0.4 | 83.2757 | 18.5057 | 306.3880 | 68.0862 |
| 2 | 22:03:03 | Night | 1.6 | 0.4 | 93.6851 | 23.4213 | 272.3449 | 68.0862 |
| 5 | 06:55:06 | Night | 1.5 | 0.4 | 99.9308 | 26.6482 | 255.3233 | 68.0862 |

*Table 1: Frequency cut-off, $f_c$, and electron density, $n_e$, calculations, from lightning strikes occurring between 16th Nov and 5th Dec 2006.*

Note: $\Delta h = h\left(\frac{\Delta f_c}{f}\right)$; $\Delta n_e = n_e\left(\frac{\Delta f_c}{f_c}\right)$; $Mean\_error = \frac{extremal\_deviations}{\sqrt{No.\_of\_measurements}}$

The average daytime ionospheric height = (69.9464 ± 11.8998) km

The average nighttime ionospheric height = (86.4759 ± 12.9807) km

### 3.2 Terminator Calculations

The narrowband files allowed graphs to be plotted in Matlab, showing changes in amplitude and phase with respect to time for the various transmitters that the AWESOME detector was monitoring.

Figure 21 shows an example of a plot, from HWU, a transmitter in Rosnay, France. Here the characteristic higher amplitude during night-time can be seen; the sunrise beginning, reaching the terminator point at around 400mins after midnight, and the daytime with lower amplitude than the night-time.

Data from a number of transmitters can be combined, and the plots compared over a number of days, as in Figure 22. There are differences in sunrise/sunset times here, which shall be examined in the next section.

[14] http://www.nssdc.gsfc.nasa.gov/space/model/models/igrf.html

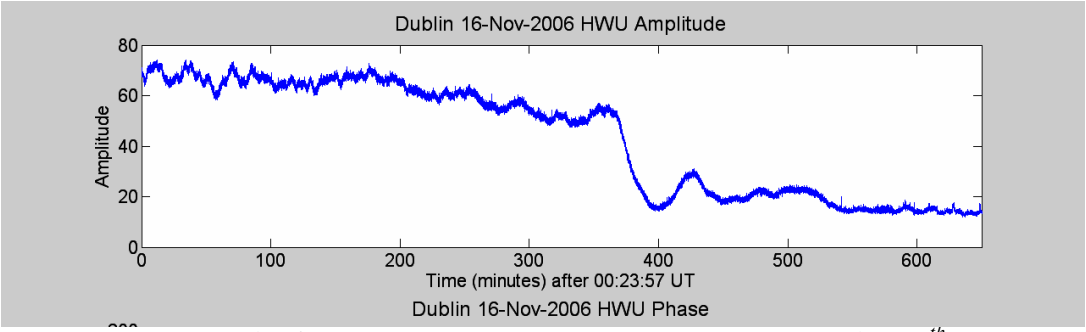


*Figure 21: Plot from transmitter in Rosnay, France, on November 16th 2006.*

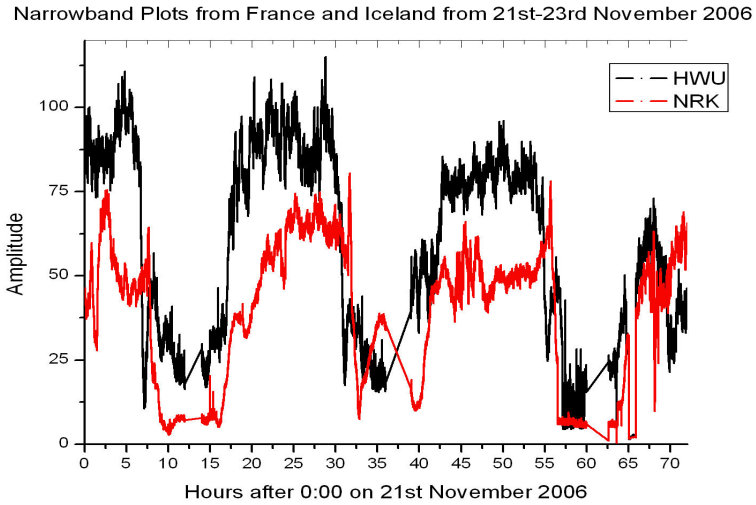


*Figure 22: Plots from transmitters at Rosnay (HWU) and Grindavik (NRK) between November 21st and 23rd 2006.*

| Transmitter | Latitude(˚) | Longitude(˚) |
|---|---|---|
| HWU | 40.7 | 1.25 |
| DHO | 53.1 | 7.6 |
| GQD | 52.71 | -3.07 |
| NAA | 44.65 | -67.3 |
| NRK | 65 | -18 |
| Dublin | 53.53 | -6.25 |

*Table 2: Latitudes and Longitudes for various transmitter locations.*

### *3.2.1 Sunrise Comparison*

In order to compare the sunrise times from the narrowband plots, and the actual values, first the actual values were calculated.

| Date Nov/Dec '06 | HWU(UT) | GQD(UT) | NAA(UT) | DUBLIN(UT) |
|---|---|---|---|---|
| 21 | 06:49 | 07:46 | 11:34 | 08:01 |
| 22 | 06:50 | 07:47 | 11:35 | 08:03 |
| 23 | 06:51 | 07:49 | 11:37 | 08:05 |
| 24 | 06:52 | 07:51 | 11:38 | 08:06 |
| 25 | 06:53 | 07:52 | 11:39 | 08:08 |
| 26 | 06:55 | 07:54 | 11:40 | 08:10 |
| 27 | 06:56 | 07:55 | 11:42 | 08:11 |
| 28 | 06:57 | 07:57 | 11:43 | 08:13 |
| 29 | 06:58 | 07:59 | 11:44 | 08:14 |
| 30 | 06:59 | 08:00 | 11:45 | 08:16 |
| 1 | 07:00 | 08:02 | 11:46 | 08:17 |
| 2 | 07:01 | 08:03 | 11:47 | 08:19 |
| 3 | 07:02 | 08:04 | 11:49 | 08:20 |
| 4 | 07:03 | 08:06 | 11:50 | 08:22 |
| 5 | 07:04 | 08:07 | 11:51 | 08:23 |
| 6 | 07:05 | 08:08 | 11:52 | 08:24 |
| 7 | 07:06 | 08:10 | 11:53 | 08:26 |
| 8 | 07:07 | 08:11 | 11:54 | 08:27 |

*Table 3: Theoretically calculated sunrise times for various transmitter locations.*

---

This was done using a JavaScript program from the US Naval Observatory.[15] The actual theoretical calculations can be found in Appendix 5.

It was necessary to know the latitude and longitude for each transmitter location, which are listed in Table 2.

Note: for latitude, a positive value indicates N, negative S and for longitude, positive is E, negative is W.

The sunrises were determined for three transmitters: France (HWU), England (GQD), and Maine (NAA), for a period of time between November 21st and December 7th 2006. Dublin's sunrise was also calculated. The theoretical sunrises are listed in Table 3.

Rather than determine the exact time of sunrise from the plots, i.e. corresponding to the above times, it was a more accurate method to determine the terminator point on the graph, i.e. the minimum point during the sunrise period (see Figure 21).

| Date | HWU(UT) | Σ(HWU) (mins) | GQD(UT) | σ(GQD) (mins) | NAA(UT) | σ(NAA) (mins) |
|---|---|---|---|---|---|---|
| 21 | 07:05 | 14 | 08:37 | 9 | 12:48 | 22 |
| 22 | 07:07 | 10 | 08:39 | 16 | 12:49 | 17 |
| 23 | 07:08 | 15 | 08:45 | 22 | 12:51 | 21 |
| 24 | 07:10 | 22 | 08:48 | 18 | 12:55 | 26 |
| 25 | 07:12 | 21 | 08:50 | 9 | 13:01 | 26 |
| 28 | 07:14 | 15 | 08:55 | 9 | 13:05 | 11 |
| 29 | 07:17 | 13 | 08:56 | 17 | 13:08 | 30 |
| 2 | 07:20 | 26 | 09:00 | 23 | 13:10 | 15 |
| 5 | 07:24 | 14 | 09:04 | 11 | - | - |
| 6 | 07:25 | 18 | - | - | - | - |
| 7 | 07:27 | 16 | 09:10 | 14 | 13:13 | 25 |
| 8 | 07:28 | 17 | - | - | - | - |

*Table 4: Terminator Times determined from Narrowband plots.*

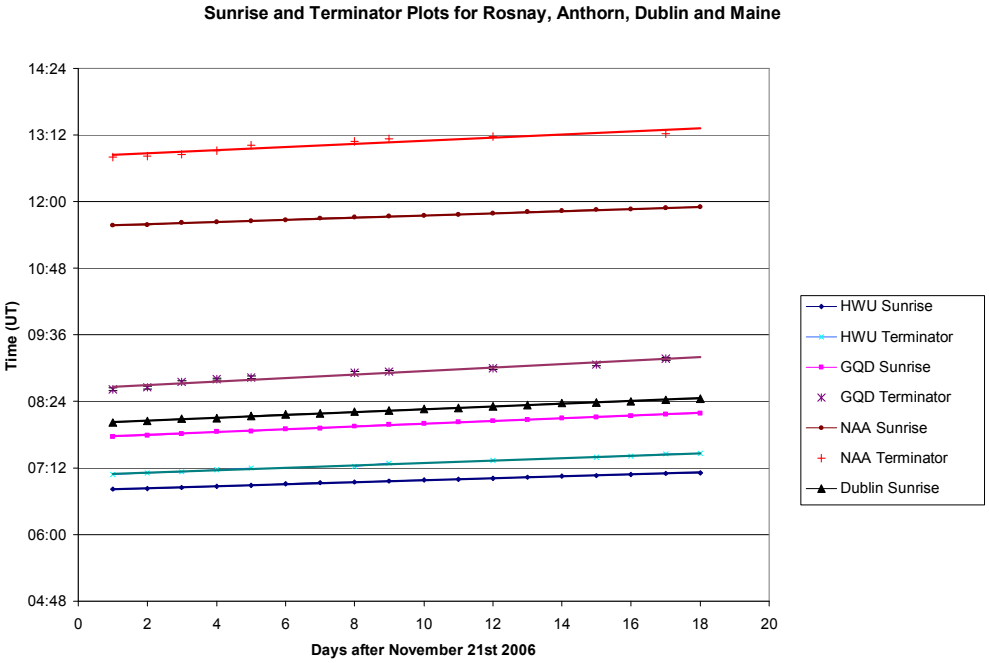


*Figure 23: Comparison of sunrise times and terminator points for Rosnay, Anthorn, Dublin and Cutler.*

The command max(data_amp) was used to determine the minimum point in Matlab, and the corresponding point of time for that minimum amplitude was then found. The terminators determined are listed in Table 4.

[15] http://www.srrb.noaa.gov/highlights/sunrise/sunrise.html

The error for the terminator was found by getting the FWHM of the curve, and then determining $\sigma = \frac{FWHM}{2.35}$.

Days that do not have a time were days where either the transmitter was shutdown or the antenna in Dublin was not taking data.

Comparing the times resulted in the plot in Figure 23. Separate plots of the different transmitters can be found in Appendix 6.

*3.2.2 Terminator Speed*

The theoretical estimation of what the terminator speed should be at Dublin, at a location 53.35°N, 6.25°W, can be found from:

Terminator Speed $= \frac{2\pi r}{t}$, where r = radius of Earth

Circumference at equator = 6378.137 km

Therefore, 2πr = circumference at Dublin $= 2\pi(6378.137)(\cos 53.35°) = 23{,}921.79 km$

t = 24 hours, the period of Earth's rotation

Therefore, Speed = 276.87 m/s

To estimate the terminator speed from the plots, the following method was used:

The waveguide was pictured to be similar to Figure 24.

Here B and C are two transmitter locations, A is a receiver in-between the two (e.g. Dublin), E is a location between A and B, D is a location between B and C. The lines EG and FH are heights of the ionosphere.

Taking an example, let A be Dublin, B be HWU, C be NRK.

Δt will be the terminator time difference between the transmitters and Dublin.

The radio wave travels along the distance (BH + HA) for Dublin to HWU, and (AG + GC) for Dublin to NRK.

So to get these distances, one needs EG and FH, and the ground distances AE, EB, BD, DC.

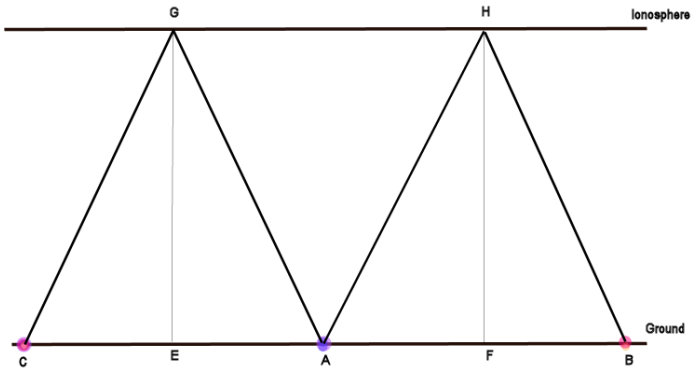


*Figure 24: Image depicting the typical path of a radio wave, reflecting off the ionosphere as it travels from one transmitter to another.*

| | DUB | GQD | HWU | NAA |
|---|---|---|---|---|
| DUB | | 224 | 1516 | 4417 |
| GQD | 224 | | 1375 | 4641 |
| HWU | 1516 | 1375 | | 5456 |
| NAA | 4417 | 4641 | 5456 | |

*Table 5: Distance between locations in km.*

---

The average height for the daytime calculated from earlier, (69.95 ± 11.90) km, was taken to be the height, as the D layer starts forming again when sunrise begins.

Points D and C were taken to be at various locations: halfway between the two points, one quarter of the way there, and one third of the way there. The distances BH, HA, AG, GB were then calculated from the right-angled triangle rule.

Then the speed = (distance BH + HA)/(difference between the terminator times)
Or speed = (AG + GB)/(terminator difference)

The distances between the various transmitters locations were needed, which were found using a mapping program called Pizza[16] (the theoretical calculation can be found in Appendix 7) with the latitude and longitudes of the locations (see Table5).
For height h = 69.95±11.90km, and using t = difference between terminator times found in Table 4, the terminator speed was calculated for different dates. Various transmitters were used: 1)GQD and HWU, 2)GQD and NAA, and 3)HWU and NAA.

[16] http://tonnesoftware.com/pizza.html

| Date(Nov/ Dec '06) | $v_{Halfway\ between}$ (m/s) | $\Delta v_{Halfway\ between}$ (m/s) | $v_{1/3\ way\ there}$ (m/s) | $\Delta v_{1/3\ way\ there}$ (m/s) | $v_{1/4\ way\ there}$ (m/s) | $\Delta v_{1/4\ way\ there}$ (m/s) |
|---|---|---|---|---|---|---|
| 21 | 250.3802 | 48.6400 | 250.5384 | 48.6707 | 250.7997 | 70.7622 |
| 22 | 250.3802 | 70.6438 | 250.5384 | 70.6885 | 250.7997 | 90.7868 |
| 23 | 237.4740 | 90.6350 | 237.6241 | 90.6922 | 237.8719 | 96.0999 |
| 24 | 235.0508 | 95.9391 | 235.1993 | 95.9997 | 235.4447 | 71.5637 |
| 25 | 235.0508 | 71.4440 | 235.1993 | 71.4892 | 235.4447 | 54.8629 |
| 28 | 228.0691 | 54.7712 | 228.2132 | 54.8058 | 228.4512 | 71.1271 |
| 29 | 232.6766 | 71.0081 | 232.8236 | 71.0530 | 233.0664 | 114.8770 |
| 2 | 230.3498 | 114.6848 | 230.4954 | 114.7573 | 230.7358 | 55.9657 |
| 5 | 230.3498 | 55.8721 | 230.4954 | 55.9074 | 230.7358 | 64.7844 |
| 7 | 223.6406 | 64.6761 | 223.7819 | 64.7169 | 224.0153 | 70.7622 |

*Table 6: Terminator Speeds for GQD and HWU*

1) GQD and HWU

Distance between them: 1375km

Ground Distance halfway between them: 687.5km

Ground one third distance: 458.33km, 2/3 distance: 916.67km

Ground one quarter distance: 343.75km, ¾: 1031.25km

The calculated terminator speed for these locations can be found in Table 6.

Note: $\Delta speed = (speed)\left(\frac{\Delta t}{t} + \frac{\Delta h}{h}\right)$

2) GQD and NAA

Distance between them: 4641km

Distance halfway between them: 2320.5km

One third distance: 1547km, 2/3 distance: 3094km

One quarter distance: 1160.25km, ¾: 3480.75km

3)HWU and NAA

Distance between them: 5456km

Distance halfway between them: 2728km

One third distance: 1818.67km, 2/3 distance: 3637.33km

One quarter distance: 1364km, ¾: 4092km

Tables 7 and 8 in Appendix 8 show the results of the terminator speed calculations for part 2) and 3).

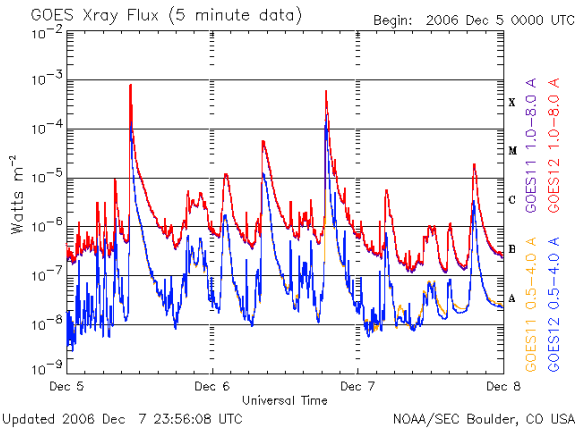


*Figure 25 (a)*

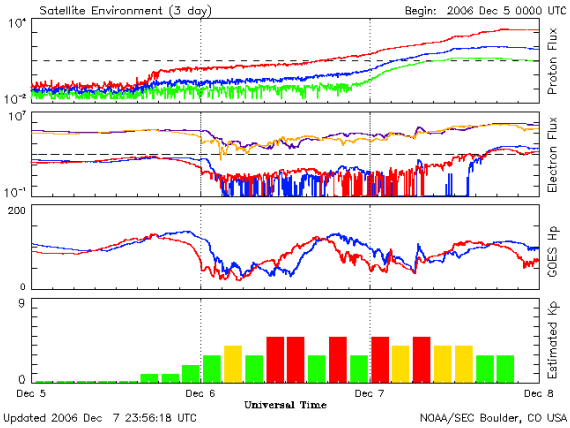


*Figure 25 (b)*

*Figure 25 shows GOES data from December 5th, 6th, and 7th 2006. 25 (a) shows Xray flux data; 25 (b) shows a Satellite Environment Plot, which combines satellite and ground-based data to provide an overview of the current geosynchronous satellite environment.*

---

### 3.3 Flares

Although this project was undertaken when the Sun was at solar minimum, solar activity increased in the final weeks of the project a number of X flares were detected.

Sunspot 10930 announced itself on December 5th 2006, with the 15th strongest flare in the past 30 years - an X9, followed by an X6 on December 6th 2006, an X3 on Dec. 13th and an X1 on December 14th 2006. A series of images showing the movement of sunspot 10930 across the sun can be found in Appendix 9.

GOES data (see Figure 25 (a)) showed the X9 flare began at 10:18a.m. UT, and peaked at 10:35 UT. Plotting GOES data with data from the receiver, showed correlation between the events, as can be seen in Figure 26. Figure 27 includes data from NLK, to compare results from day and night.

The flares at the transmitters began 8mins after 10:18 UT, at 10:26am. Comparing this with the distance from the Sun to the Earth, and the speed of light:

$$Time = \frac{Dis\tan ce}{Speed} = \frac{1.49x10^8\,km}{3x10^8\,m/s} \sim 8\min s\,.$$

Peaks occurred in the graphs at 10:33am UT for HWU, 10:31 UT for NRK and 10:36 UT for NAA.

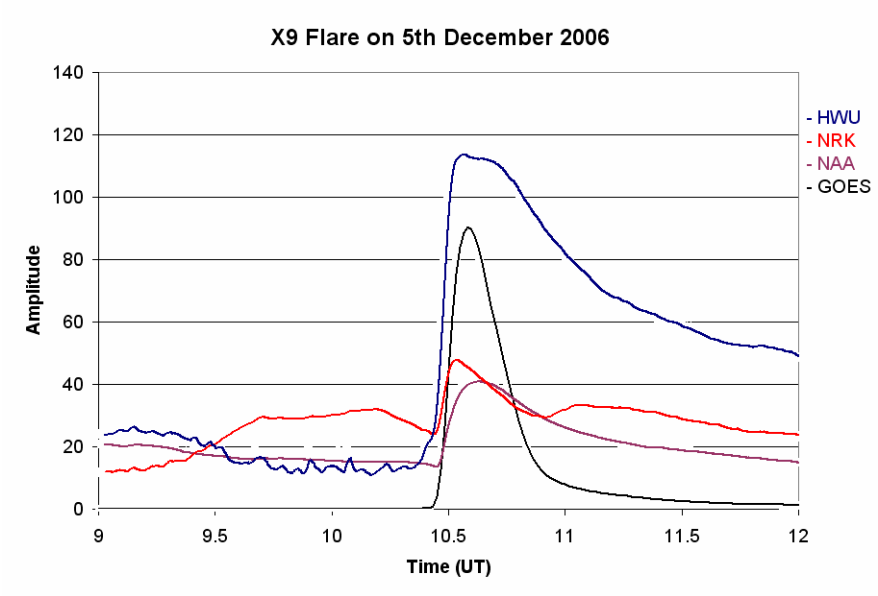


*Figure 26: Peaks on narrowband plots showing flare effecting monitors in France, Iceland, and Maine. GOES plot is superimposed for comparison.*

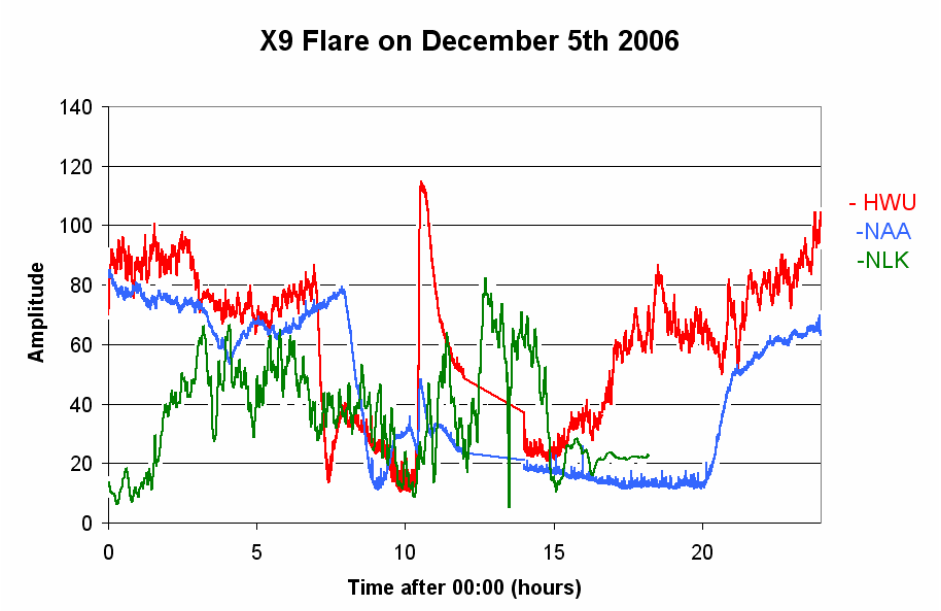


*Figure 27: Plots from Rosnay, France, Cutler, Maine, and North Dakota, on 5th December 2006.*

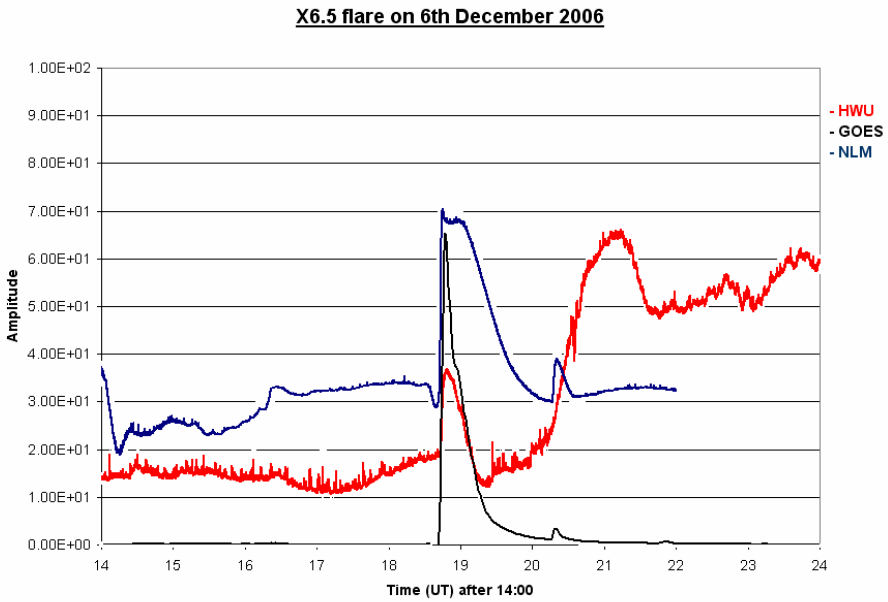


*Figure 28: Plots from Rosnay, France and North Dakota, USA, with GOES data superimposed, showing the X6.5 flare of the December 6th 2006.*

---

On December 6th 2006, an X6.5 flare began at 18:29 UT, and peaked at 18:47 UT. Peaks in the narrowband plots occurred at 18:50 UT for HWU, 18:55 UT for NLM, as can be seen in Figure 28.

This flare occurred at night-time in Ireland, so it was necessary to compare the plot with a transmitter that was located in an area which had its daytime during the flare. NLM was looked at, which is located in North Dakota, USA (see Figure 28).

CMEs were hurled into space by the X flare's explosions. This delivered glancing blows to Earth's magnetic field as early as December 7th 2006, producing high-latitude geomagnetic storms. Based on the energy and number of solar protons streaming past Earth, NOAA ranked the storm as category S3.[17]

After three days of intense storming, sunspot 10930 suddenly went quiet on the 10th. The sunspot's magnetic field settled into a stable configuration and posed little threat for strong solar flares. However on the December 13th 2006, an X3 flare occurred. Sunspot 10930 unleashed an X3 flare at 02:14 UT, peaking at 02:40 UT (see Figure 29 (a)).

---

[17] http://spaceweather.com

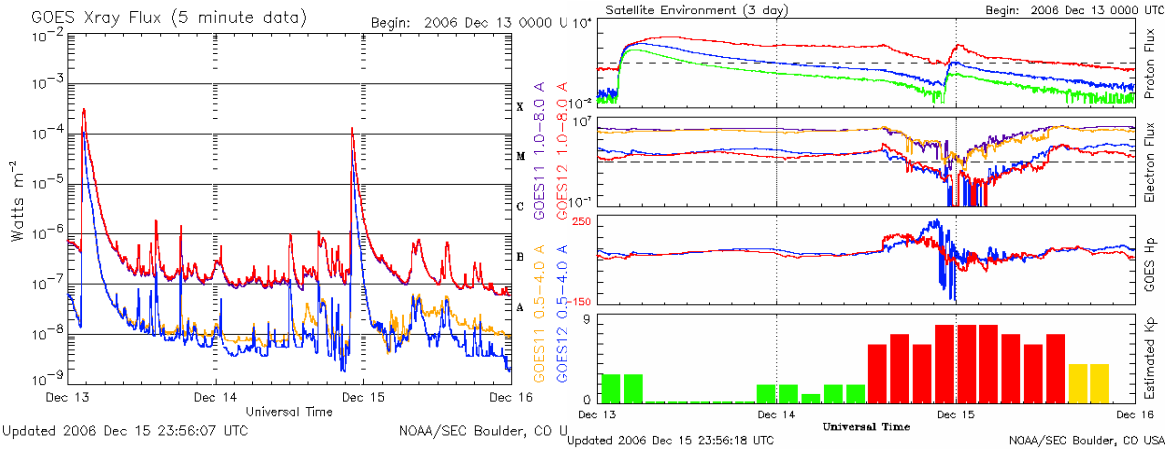


*Figure 29 (a)* *Figure 29 (b)*

*Figure 29 shows GOES data from December 13th- 15th 2006. 29 (a) shows Xray flux data; 29 (b) shows a Satellite Environment Plot.*

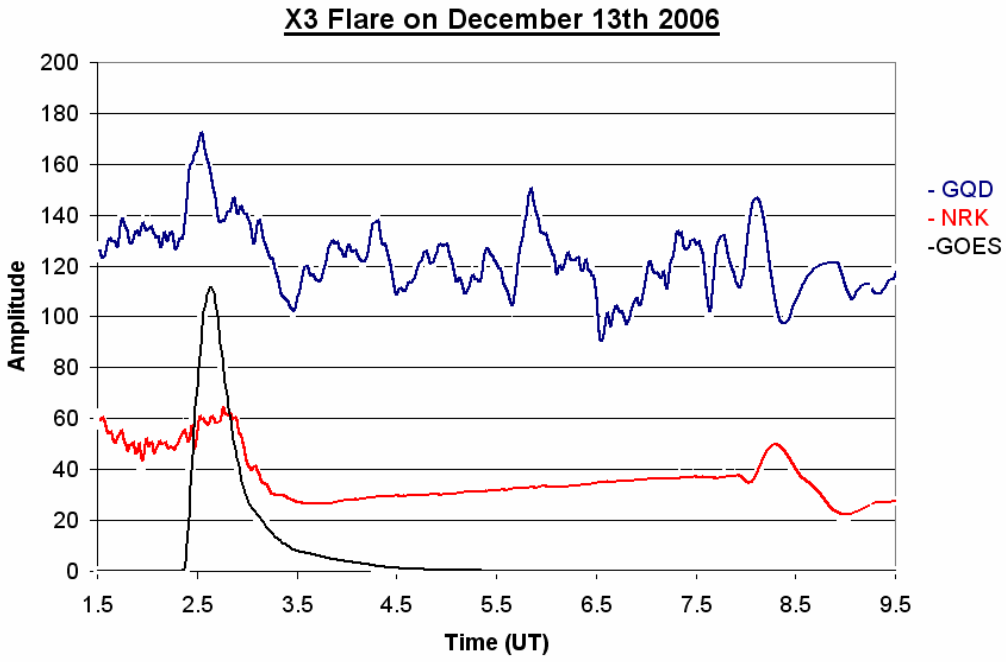


*Figure 30: Plot of GOES data, and data from Iceland and England, on December 13th 2006.*

*Figure 31: Image of the Northern lights off the coast of Northern Ireland. Taken by Martin Mc Kenna, Conor Mc Donald, Jonathan Bingham.*[18]

---

Again, the antenna detected the flare 8mins after the event began, as seen in Figure 30, but as it was during our night-time the data plots were not very clear.

As a result of the X3 blast another radiation storm occurred. Based on the energy and number of solar protons streaming past Earth, NOAA ranked the storm as category S2. The explosion hurled a coronal mass ejection toward Earth, which hit Earth on December 14th 2006, at approximately 14:00 UT. Earth's magnetic field reverberated for more than 24 hours after the impact. It caused strong geomagnetic storms, sparking Northern Lights which could even be visible in Ireland (see Figure 29 (b)).

Another flare X1.5 flare occurred on December 14th 2006, starting at 21:07 UT; peaking at 22:15 UT. The Dublin software had crashed, but other receivers worldwide picked it up.

The X1 flare launched another CME, but it did not cause such a widespread display. The blast was not squarely Earth-directed, so the CME's impact was only a glancing one. However the aurora was still visible in the Northern latitudes.

The sun's rotation carried the active region toward the western limb, where it vanished on December 18th 2006. Solar activity then returned to low levels, typical during the solar minimum.

---

[18] Astronomy Ireland 2006

| Date | Time(UT) | Flare Class | $F_s^o$ | $F_s^f$ | $N_e^o(cm^{-3})$ | $N_e^f(cm^{-3})$ | $N_e^f/N_e^o$ Ratio |
|---|---|---|---|---|---|---|---|
| 5th Dec | 10:35 | X9 | 1.26E-04 | 9.06E-04 | 50238 | 134715.5 | 2.68 |
| 6th Dec | 18:47 | X6.5 | 1.38E-04 | 6.31E-04 | 1861 | 3979.44 | 2.14 |
| 13th Dec | 02:40 | X3 | 9.135E-05 | 3.41E-04 | 1719 | 3321.23 | 1.93 |
| 14th Dec | 22:15 | X1.5 | 1.003E-04 | 1.52E-04 | 1719 | 2116.15 | 1.23 |

*Table 7: Electron Densities of the ionosphere for various X class flares detected.*

---

*3.3.1 Electron Density During the flares*

At an altitude of about 110 km, for an observed flare-induced electron density 1.5 times the pre-flare value:

$$F_s^f / F_s^o = \left( N_e^f / N_e^o \right)^2 = (1.5)^2 = 2.25$$ [Mendillo et. al. 2006]

The general pre-flare value for electron density would be in the $10^3$ $cm^{-3}$ range for 110km during the day, and $10^2$ $cm^{-3}$ at night.

Values for $F_s^0$ and $F_s^f$ were taken from GOES data, and values for $N_e^o$ were taken from the International Reference Ionosphere, 2001.[19]

# CHAPTER 4: DISCUSSION AND CONCLUSIONS

## 4.1 Terminator Calculations

The plots obtained from this project are very typical to what one might expect from an ionospheric monitor. In Figure 21 the amplitude is much higher at night-time, then, as sunrise occurs, there is a sharp drop in amplitude, followed by a steadying out, and then the daytime signal stays much lower than that at night.

The reflection of the waves in the layers of the ionosphere varies. The ionisation density of the D layer (~$10^2$ electrons/$cm^3$) is not enough to reflect the VLF waves, so during the day the waves pass through the D layer and are reflected by the higher ionised E and F layers. However the D layer is partially ionised and so attenuates the signal somewhat. At night in the absence of solar radiation, the D layer disappears. So the VLF waves are reflected by the E and F layers, and the signal strength is greater due to the lack of D layer to attenuate the signal.

In the plots of the flares, as in Figure 26, a peak occurs when the flare occurs. When a SID occurs, the D layer becomes very highly ionised, and so this layer can reflect the VLF waves. The signal strength increases as the wave has less distance to travel, and it doesn't have to pass through a lightly ionised layer. As soon as the X-rays end, the SID or radio black-out ends as the electrons in the D region recombine rapidly and signal strengths return to normal [Kelley & Heelis 1989].

### *4.1.1 Sunrise Times*

The times for the terminators agree well with what would be expected, with the sunrise occurring in France first, then England, and finally Maine, as the terminator moves its way across the Earth in a westward direction. If there were more time for the project, one would have noticed the sunrise times continuing to gradually increase until December 22nd 2006, the winter solstice. This day is one of the two events of the year when the sun is at its greatest distance from the equatorial plane. After that day one would have observed the sunrise times decreasing, until the next solstice, the

[19] http://modelweb.gsfc.nasa.gov/models/iri.html

summer solstice of June 21st 2007. Rather than see a linear plot as in Figure 23, one would have seen a curve, initially increasing, and then decreasing.

### 4.2 Sferics

The sferics found in the spectra obtained were consistent with what might be expected. Sferics are impulsive signals emitted by lightning. When a lightning strike occurs, 0.1% of the energy is released in the form of electromagnetic waves. Most of the EM wave energy is focused in VLF and ELF frequencies. The VLF energy is guided by the Earth's waveguide, bouncing off the ionosphere. It has very low attenuation (1-3 dB per 1000 km) so signals can be detected halfway around the world. The dynamic spectra of sferics are characterized by vertical lines indicating the simultaneous arrival of all audio frequencies.

The calculations for the cut-off frequency determined the ionospheric height to be 69.95±11.90km during the day and 86.48±12.98km at night. This agrees, within the limits of error, with the expected heights for day and night of ~75km and 85km respectively. [Cohen 2006]

Examining the results in Table 1, the density at night for this height range is lower than during the daytime. The values for the heights found would be around the D layer values, so one would expect the density in these regions to drop at night-time, as the D layer disappears at night.

Also, looking at all the electron density values, there are ~$10^3$electrons/$cm^3$ in the range ~ 60-100km, which is to be expected comparing these values to the typical ionospheric model, such as in Figure 5.

It would have been nice to have a wider range of results for the ionospheric heights and corresponding electron densities. One may then have been able to plot ionospheric height vs. electron density and compare that to Figure 5. However, the results were too close together for that, with a small range of times and heights. This was due to the noisiness of the spectrum near the cut-off frequencies.

Even so the sferic in the spectra were consistent with what might be expected. Perhaps the number of lightning strikes during a day could have been monitored as well, comparing to weather forecasts, and trying to determine the location of the lightning strikes. I would certainly think it would be a good project for the future if one could move the antenna to a quieter location.

### 4.3 Flares and CMEs

Each of the flares was detected on Earth exactly 8mins after a sudden X-Ray increase was detected on GOES, which was to be expected.

An ejection from the Sun includes intense UV and X-ray radiation, also radio waves, and sometimes high-energy particles can be sent out of the Sun. The energetic radiation travel at the speed of light, and so arrive at Earth just 8mins after leaving the flare site, well ahead of any particle or coronal materials [Alex et al. 2003]. The energetic particles, x-rays and magnetic fields from these solar flares bombard the Earth in geomagnetic storms.

So what the AWESOME antenna picked up was the effect of the X-Rays. The flares caused extra penetration of the X-Rays through the different layers of the ionosphere, increasing the electron density, causing more reflection of radio waves, and hence a signal increase. The UV radiation would have been absorbed by the higher up layers.

However, changes in proton and electron fluxes could also be seen from GOES data, not straight away but days after the flares occurred. This is the effect of the Coronal Mass Ejections.

CME's disrupt the flow of the solar wind and produce disturbances that strike the Earth. It ejects material consisting of plasma, consisting primarily of electrons and protons (in addition to small quantities of heavier elements such as helium, oxygen, and iron), plus the entrained coronal magnetic field.[20] This increases the density and pressure of the solar wind and produces a shock wave similar to a sonic boom.

When the solar cloud reaches the Earth as an ICME (Interplanetary CME), it may disrupt the Earth's magnetosphere, compressing it on the dayside and extending the night-side tail. When the magnetosphere reconnects on the night-side, it creates trillions of watts of power, which is directed back towards the Earth's upper atmosphere.[18] This process can cause particularly strong aurora.

Normally the geomagnetic field protects the Earth from the sun's emissions, providing an invisible barrier to the charged particles that stream towards the planet. This is due to the magnetic field's ability to reflect the charged particles. But during periods of intense solar activity, the geomagnetic flow from the sun is much stronger.

[20] http://en.wikipedia.org/wiki/Coronal_mass_ejection

These magnetic storms produce spectacular displays of the Aurora Borealis and the Aurora Australis.

When, e.g. an ICME, impacts the Earth's magnetosphere, it temporarily deforms the magnetic field, which changes the direction of compass needles and induces large electrical ground currents in Earth itself. ICME impacts can induce magnetic reconnection in the magnetotail. This then launches protons and electrons downward toward the Earth's atmosphere, where they form the aurora.
During a geomagnetic storm the F2 layer will become unstable, fragment, and may even disappear completely.

Protons are accelerated in shock waves at the leading-edge of CMEs, so when the proton count rises, as one can see in Figures 25 (b) and 29 (b), one can guess that a CME is en-route. In the case of the solar activity on December 5$^{th}$ and 6$^{th}$ 2006, this may have caused auroras in the Northern latitudes if the CME hit the Earth on the December 8$^{th}$ or 9$^{th}$ 2006, however this time it missed the Earth. This was because the sunspot's location near the limb on the December 5$^{th}$ and 6$^{th}$ meant the flares and CME were not Earth-directed, so the CME's impact was only a glancing one. From the events resulting in Figure 29 (b), the blast was Earth directed, and caused aurora in the Northern latitudes, even extending down to Ireland.

One interesting discovery from the plots of the flares obtained from the antenna, is that the antenna did not pick up the flares as strongly during the night-time as it did during the day. The flare on December 5$^{th}$ occurred during Ireland's daytime. It was also daytime at HWU, NRK and NAA, producing particularly large peaks on the plots in Figure 26. However, when one examines Figure 28, which includes a location in North Dakota, USA, which was during the night at the time of the flare, one can see that the sheer noise the antenna pick up at night 'drown out' the flare. The flare on the 6$^{th}$ occurred during our local night; however NLM had its daytime. This was also the case for the flares of the 13$^{th}$ and 14$^{th}$, they occurred during our local night. The plot in Figure 30 from the 13$^{th}$ shows the noise nearly wipes out the flares, but knowing the time of occurrence, and superimposing the GOES data, one can safely guess which are the flares and which are noise.

Solar flares are classified as A, B, C, M or X [Philips 1992] according to the peak flux (in W/m$^2$) of 1 to 8Å X-rays near Earth, as measured on the GOES spacecraft [Mewaldt et al. 2005]. Each class has a peak flux ten times greater than the

preceding one; with X class flares having a peak flux of order $10^{-4}$ $Wm^{-2}$. Energies of large flares may be as high as (1-3) x $10^{25}$J [Somov 2006].

The AWESOME antenna only seemed to pick up flares that were X class, but due to the sensitivity of the equipment one might have expected C and M class flares to be picked up also. Looking at the various flares that occurred during the period of time in which the project was carried out, it seems that many 'larger' flares took place during UT night, so the noise would have drowned out many of them. Daytime flares were mainly A and B class, which may be too small to pick up anyway, especially with the background noise interference that the antenna experienced at its location on the roof.

The calculations of electron densities seemed showed typical increases due to the effect of the flares. One would expect a larger increase in density for the lower D level, with more X-ray penetration, with and increase in E and F layers as well, but not as significant. The results from this project were for heights that corresponded to the D layer, with the densities approximately doubling. The increase in the densities also seemed to decrease with the class of the flare. Comparing to other research this agrees well; Mendillo et.al. discovered a 2.25 times increase at 110km, and Tsurutani et. al. determined a ~30% increase for the 28$^{th}$ October 2003 flare. However some research has recorded increases of up to 200% [See Afraimovich et al 2001]. Thus a clearer picture would need to be obtained, i.e. effects on a larger range of heights of a greater number of flares would need to be examined before a clear judgement could be made.

The results of this project in general are consistent with theory and other research. The suggestion I would make would be that even better results could be obtained, monitoring over a longer time scale, and in a location that was not as noisy.

# REFERENCES

AIPD Correspondance Course Programme, Radio Wave Propagation and Antennas.

Afraimovich, E. L., Altyntsev, A. T., Kosogorov, E. A., Larina, N. S., Leonovich, L. A., 2001, JATP, 63, 17, 1841-1849(9).

Ajabshirizadeh, A., Filipov, B., 2004, Sol. Phy., 221, 283–295.

Alexa, S., Mukherjeea, S., Lakhina, G. S., 2006, JATP, 68, 7, 769–780.

Antiochos, S. K., DeVore, C.R., Klimchuk, J.A., 1999, ApJ, 510, 485–493.

Arge, C.N., Harvey, K.L., Hudson, H.S., Kahler, S.W., 2003, in AIP Con. Proceedings 679, Solar Wind Ten, ed. Velli, M., Bruno, R., Malara, F., (Melville, NY), 202.

Barr, R., Llanwyn Jones, D., Rodger, C. J., 2000, JATP, 62, 1689-1718.

Boithais, Lucien, Radio Wave Propagation, McGraw Hill 1987.

Cohen, Morris, 2006, Very Low Frequency Group, Stanford University.

De Pontieu, B., Erdélyi, R., Stewart, J., 2004, Nature, 430, 536–539.

Fisk, L. A., 2003, Nature, 426, 21-22.

Forbes, J. M., Bruinsma, S., Lemoine, F. G., 2006, Science, 312, 1366-1368.

Gallagher, P., Moon, Y., Wang, H., 2002, Sol. Phy., 209, 1, 171-183.

Galperin, Y. L., 1995, JATP, 57, 12, 1397-1414.

Giacalone, J., Jokipii, J.R., 2001, Adv. Space Res, 27, 3, 461-469.

Green, J., The Magnetosphere, SSDOO Education Resources, 2004.

Howard, R.A. et al., 1997, Coronal mass ejection, 99, 35, 17-26.

Kelley, M. C., Heelis, R. A., The Earth's Ionosphere: Plasma Physics and Electrodynamics, Academic Press, 1989.

Krimigis, S. M. et al. 2003, Nature, 426, 45 - 48.

Lilesten, J., Bornarel, J., Space Weather, Environment and Societies, Springer 2006.

Manchester, W. B., Ridley, A. J., Gombosi, T.I., DeZeeuw, D. L., 2005, AdSpR, 38, 2, 253-262.

Marsch, E., 2005, AdSpR 38, 5, 921-930.

Mendillo, M., Withers, P., Hinson, D., Rishbeth, H., Reinisch, B., 2006, Science, 311, 5764, 1135-1138.

Mewaldt, R.A. et al, 2005, American Geophysical Union, Spring Meeting 2005, abstract #SH32A-05.

McDonald, F. B. et al., 2003, Nature, 426, 48–50.

NOAA: Geomagnetism, National Geophysical Data Centre, April 2005.

Ohya, H., Nishino, M., Murayama Y., Igarashi K., 2003, Earth Planet Space, 55, 627-635.

Okada T., Iwai, A., Natural VLF Radio Waves, Wiley 1988.

Parker, E.N., 1998, ApJ, 128, 664-676.

Phillips K. J., Guide to the Sun, Cambridge University Press, 1992.

Phillips S., Exploration: The Atmosphere, NASA Portal, 1995.

Plunkett, S.P., et. al., 2000, Sol. Phy., 194, 371-391.

Reames, D. V., 2004, AdSpR, 34, 381–390.

Roach J., Why does the Earth's Magnetic Field Flip?, National Geographic, Sep 27 2004.

Russell, C. T., SSC Space Physics Tutorial, UCLA, 2000.

Schatten, K. H. 2003, AdSpR, 32, 4, 451-460.

Schwabe, H. R., Solar Observations During 1843, Astronomische Nachrichten, 20, 495.

Smith, C. W., Bieber, J. W., 1991, ApJ, 370, 435-441.

Somov, B. V., 2006, Solar System Research, 40, 2, 85–92.

Svennesson, J., Westerlund, S., 1979, JATP, 41, 4, 361-365.

Thierry Alves, Simple Earth-Ionoshere Waveguide Calculation, 24 Aug 2003

Tsurutani, B. T., Mannucci, A. J., Iijima, B., Guarnieri, F.L., Gonzalez, W. D., Judge, D. L.,Gangopadhyay, P.,Pap, J., 2006, AdSpR,37, 1583 – 1588.

U.S Navy Antenna theory training material used for a better understanding of Wave Propagation.

Webb, D. F., 2000, JATP, 62, 1415-1426.

Welch C., solcomhouse.com, Originally from US Weather Service.

Yohkoh mission, NASA, Jan 13, 199

# APPENDIX 1

---

**Equipment list:**

- Pre-amplifier box, weather-proofed with aluminium
- Preamplifier cards
- Line receiver box
- Filter cards for line receiver
- Two pre-looped 2.6m air-core magnetic antenna wire, three pin connectors at end of each (1ohm, 1mH)
- Signal 14pin connector cable
- NIDAQ 6034E PCI card
- Shielded 68pin to 50pin cable for PCI card
- VIC 100 timing GPS antenna
- N-type GPS cable
- Nullmodem 9pin serial cable
- Power cord for line receiver

For antenna mount:

- 5 lengths 1.3m 1” PVC piping (Durapipe MTS 1 UPVC Class E Tube)
- 5way 1” PVC cross piece (from 1 100 Durapipe PVC Socket and 1 122 Durapipe PVC Tee)
- 1” socket and bolt for detractable length (1 100 Durapipe PVC Socket)
- 4” bolt, nut and washer

# APPENDIX 2:
# Software Settings for VLF_DAQ Console

---

*Station Information:*
Station ID: DB
Address: Trinity College Dublin, Ireland

*FTP Settings:*
FTP Name: Dublin
Host IP Address: vlf-europe.stanford.edu
Host Port No: 21
Username: hail
Host Data Directory: VLFData
FTP file starting: 12:00, ending at 14:00

*Filter Settings:*
Unique filter name: NB
Filter from file:
C:\VLF_DAQ\filters\nb_filter.dat

*Spectrogram:*
Min dB: 22, Max dB: 118
Host IP Address: nova.stanford.edu
Host Port Number: 21
Username: vlf
Host data directory:
public_html/hardware/fieldsites/dublin
JPEG Quality: 50

*Broadband Acquisition Settings*:
Sample Frequency: 100KHz
Primary Filter: NONE
A/D Card: ADC
A/D Channels: N/S and E/W
Start 0:50
End: 23:55
Period: 0:10

*Narrowband Acquisition Settings:*
Primary filter: NB
Sample Frequency: 50Hz
Acquisition times were set starting at 15:00 and ending at 12:00

# APPENDIX 3:

# Layout of data in .mat file

---

VERSION
station_name
station_description
antenna_bearings
antenna_description
computer_sn
gps_sn
hardware_description
adc_type
adc_sn
adc_channel_number
Fs
filter_taps
is_broadband
call_sign
Fc
is_msk
cal_factor
is_amp
latitude
longitude
altitude
gps_quality
start_year
start_month
start_day
start_hour
start_minute
start_second
data

# APPENDIX 3(a):
# Manual fft command

---

```
dataFFT = fft(data-mean(data), 1E5+1);
plot(0:5E4, 20*log10(abs(dataFFT(1:(5E4+1)))))
```

---

# APPENDIX 3(b):
# Manual Plot Command

---

```
% First file
load filename1.mat  % loads the data into Matlab
starttime1 = start_hour + 60*start_minute + 60*60*start_second; % time of the first
recording, in hours UT
data1 = data;
clear data;

% Second file
load filename2.mat  % loads the data into Matlab
starttime2 = start_hour + 60*start_minute + 60*60*start_second;  % time of
the second recording, in hours UT
data2 = data;
clear data;

%Repeat above as many times as needed

figure;
plot((1:length(data1))/60/60+starttime1,data1,(1:length(data2))/60/60+starttime2,data
2)  % append with more as needed
```

# APPENDIX 4:

## Spectra of Sferics picked up from the AWESOME antenna.

---

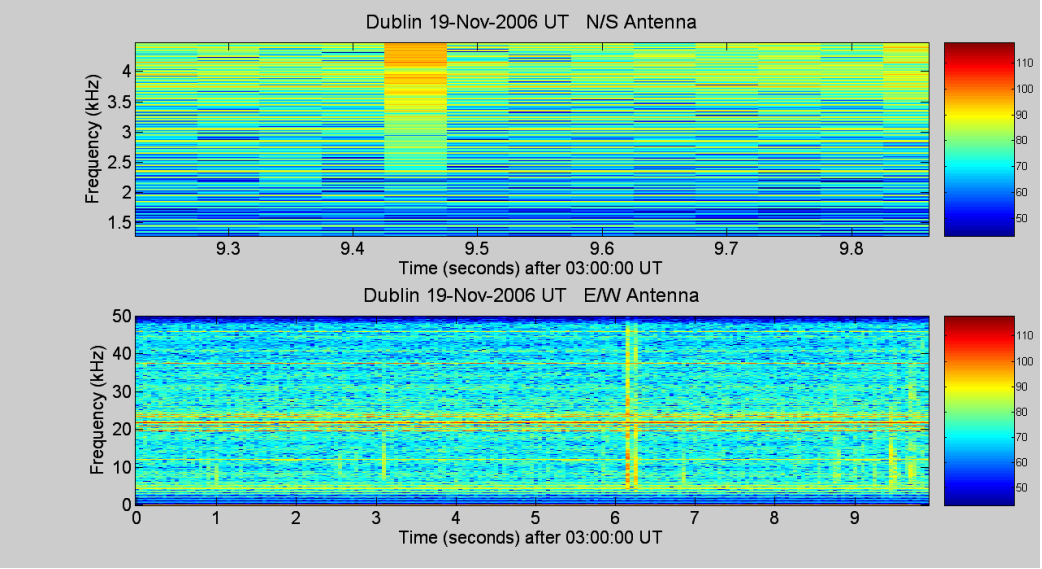


*Figure 32: Sferic at 03:00:06UT on 19th November 2006.*

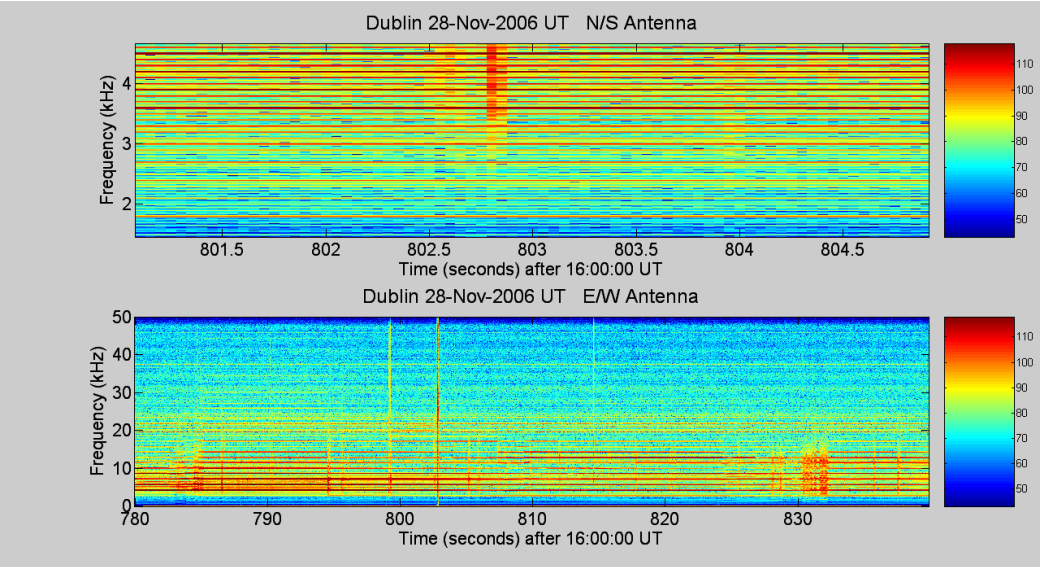


*Figure 33: Sferic at 16:13:10UT on 28th November 2006.*

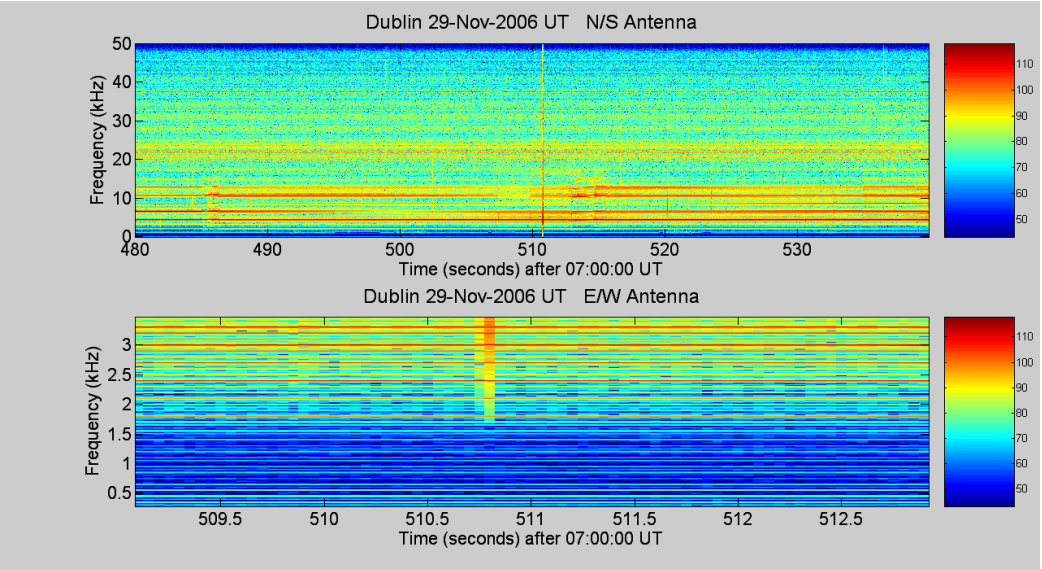


*Figure 34: Sferic at 07:08UT on 29th November 2006.*

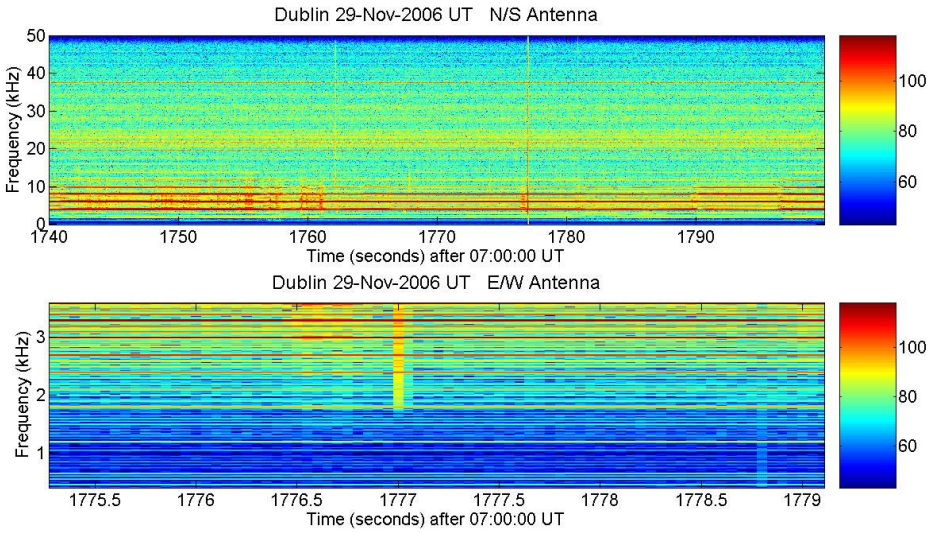


*Figure 35: Sferic at 07:29:37UT on 29th November 2006.*

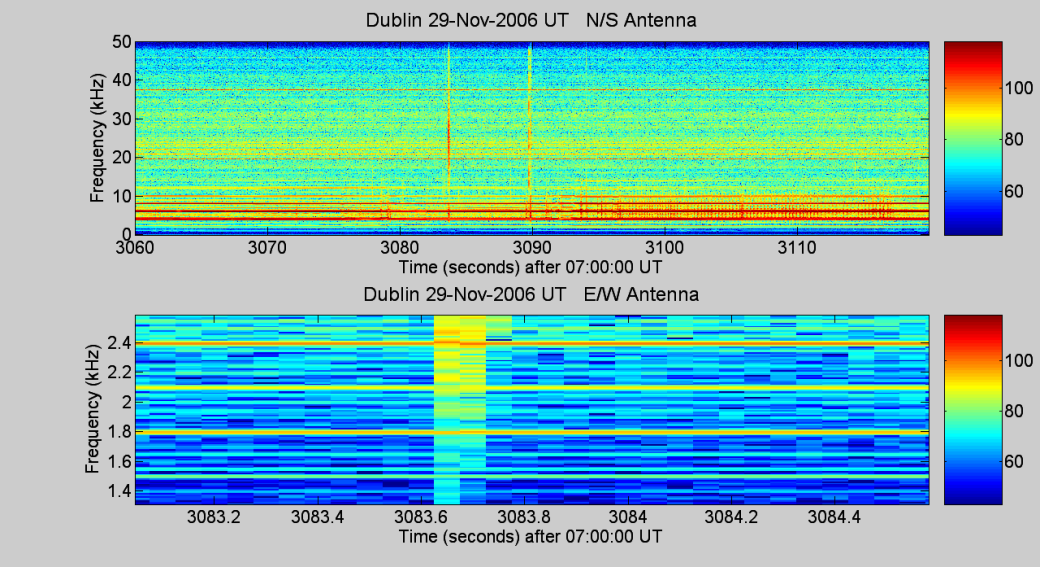


*Figure 36: Sferic at 07:51:24UT on 29th November 2006.*

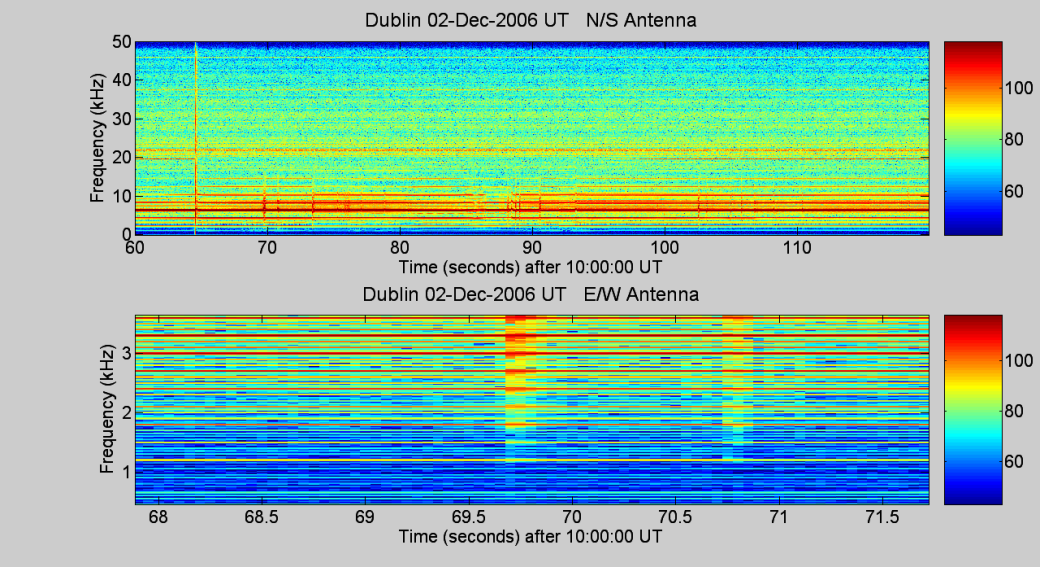


*Figure 37: Sferic at 10:01:09UT on 2nd December 2006.*

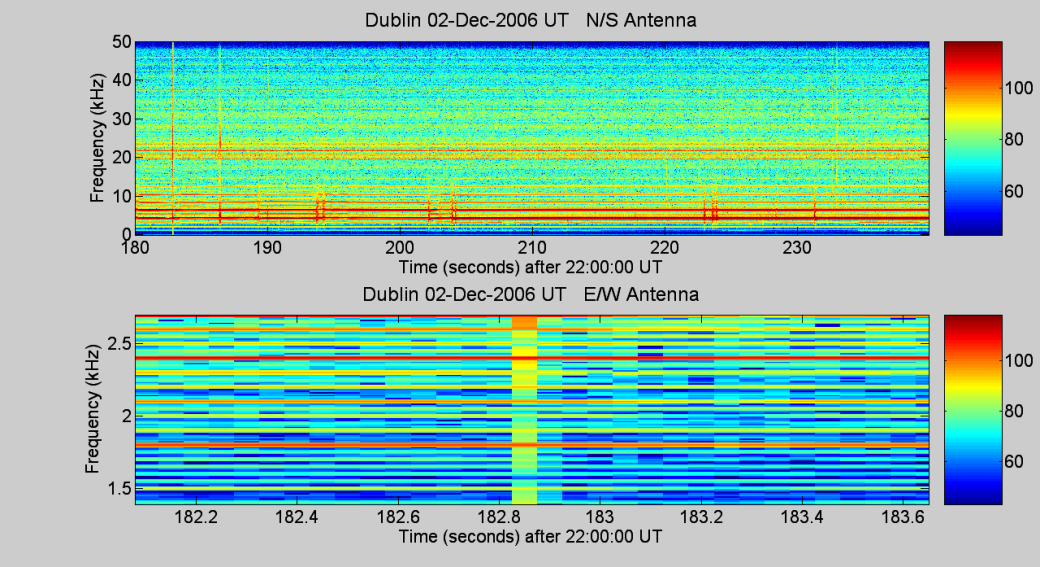


*Figure 38: Sferic at 22:03:03UT on 2nd December 2006.*

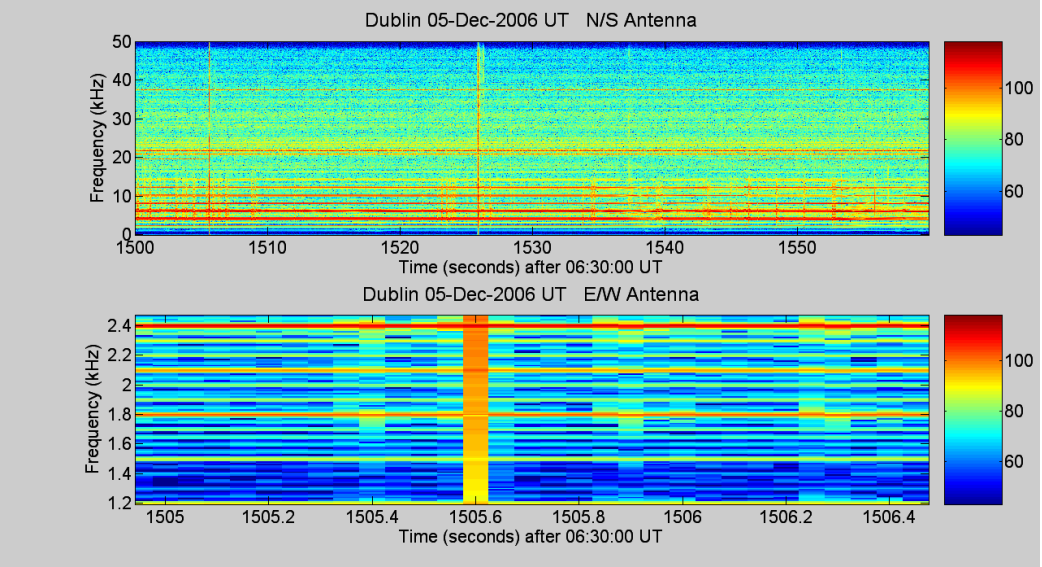


*Figure 39: Sferic at 06:55:06UT on 5th December 2006.*

# APPENDIX 5:

# Calculation of Sunrise Time for Various Latitudes.

[Cornwall et. al. 2006][21]

---

## General Solar Position Calculations:

First, the fractional year (γ) is calculated, in radians.

$$\gamma = \frac{2\pi}{365}(day\_of\_year - 1 + \frac{hour - 12}{24}$$

From γ the equation of time (in minutes) can be estimated, and the solar declination angle (in radians):

$$eqtime = 229.18 * (0.000075 + 0.001868\cos\gamma - 0.032077\sin\gamma - 0.014615\cos 2\gamma - 0.049849\sin 2\gamma)$$

$$decl = 0.006918 - 0.399912\cos\gamma + 0.070257\sin\gamma - 0.006758\cos 2\gamma + 0.000907\sin 2\gamma - 0.002697\cos 3\gamma + 0.00148\sin 3\gamma$$

Next, the true solar time is calculated. First, the time offset is found (in mins), then the solar time (mins):

$$time\_offset = eqtime - 4(longitude) + 60(timezone)$$

Where eqtime is in mins, longitude in degrees, timezone in hours from UTC

$$tst = hr(60) + mm + {}^{ss}\!/_{60} + time\_offset$$

Where hr is the hour (0-23), mm is the minute (0-60), ss is the second (0-60)

The solar hour angle, in degrees, is:

$$ha = \left({}^{tst}\!/_{4}\right) - 180$$

## Sunrise/Sunset Calculation:

For the special case of sunrise or sunset, the zenith is set to 90.833° (the approximate correction for atmospheric refraction at sunrise and sunset), and the hour angle becomes:

---

[21] http://www.srrb.noaa.gov/highlights/sunrise/calcdetails.html
Cornwall, C., Horiuchi, A., Lehman, C., National Oceanic and Atmosperic Administraion, Surface Radiation Research Branch, 2006

$$ha = \pm\left(\frac{\cos(90.833)}{\cos(lat)\cos(decl)} - \tan(lat)\tan(decl)\right)$$

where the positive number corresponds to sunrise, negative to sunset.

Then the UTC time of sunrise (or sunset) in minutes is:

$$sunrise = 720 + 4(longitude - ha) - eqtime$$

where longitude and hour angle are in degrees and the equation of time is in minutes.

---

# APPENDIX 6:
# Sunrise Plots for Various Transmitters

---

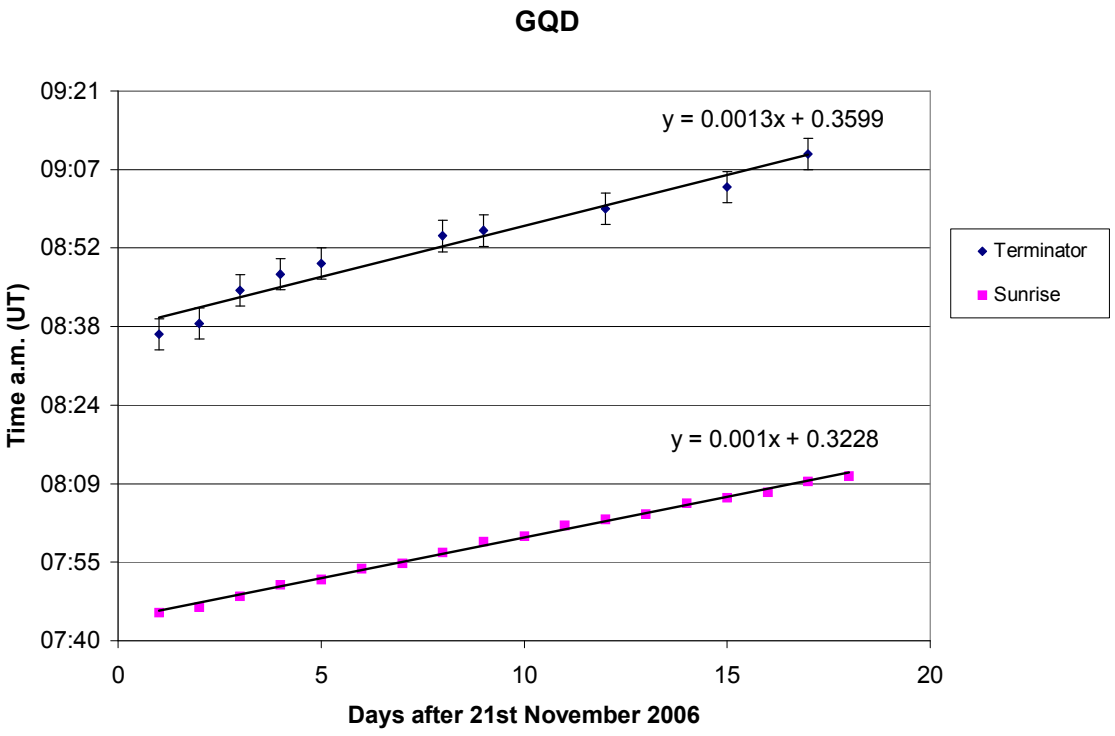


*Figure 40: Plot of Sunrise and Terminator Times for Anthorn, England, between 21st November and 8th December 2006.*

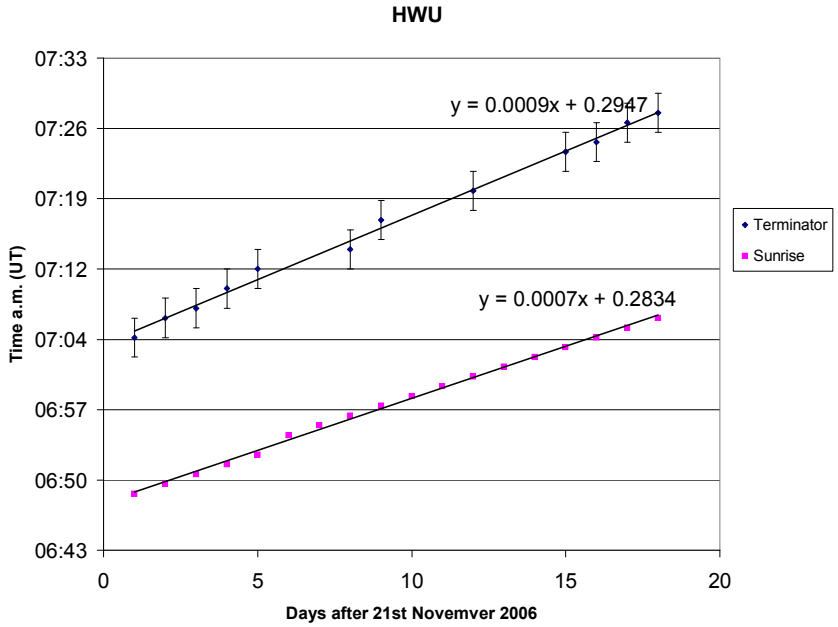


*Figure 41: Plot of Sunrise and Terminator Times for Rosnay, France, between 21st November and 8th December 2006.*

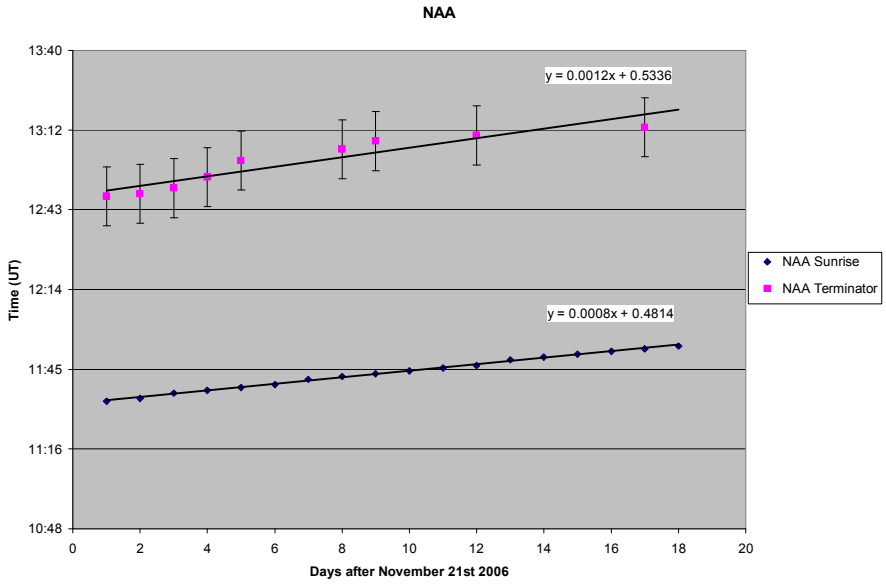


*Figure 42: Plot of Sunrise and Terminator Times for Cutler, Maine, between 21st November and 8th December 2006.*

# APPENDIX 7:

# Calculation of Distance between two Locations at different Latitudes.[22]

---

This can be calculated using Haversine's formula:

R = earth's radius (mean radius = 6,371km)

$\Delta lat = lat_2 - lat_1$

$\Delta long = long_2 - long_1$

$a = \sin^2(\Delta lat/2) + \cos(lat_1).\cos(lat_2).\sin^2(\Delta long/2)$

$c = 2.\text{atan2}(\sqrt{a}, \sqrt{(1-a)})$

$d = R.c$

(Note that angles need to be in radians to pass to trig functions).

This formula assumes a spherical earth, ignoring ellipsoidal effects. The Earth is actually oblate spheroidal, with a radius varying between about 6,378km (equatorial) and 6,357km (polar), and local radius of curvature varying from 6,336km (equatorial meridian) to 6,399km (polar). This means that errors from assuming spherical geometry might be up to 0.55% crossing the equator, though generally below 0.3%, depending on latitude and direction of travel. If greater accuracy is needed, the result can be refined by using the local radius of curvature. Errors would then be below 0.01% over smaller distances, up to about 0.1% for trans-continental distances.

[22] http://www.movable-type.co.uk/scripts/LatLong.html

# APPENDIX 8:

## Results of Terminator Speed Calulations between GQD and NAA, and HWU and NAA transmitter locations.

| Date(Nov/ Dec '06) | $v_{Halfway\ between}$ (m/s) | $\Delta v_{Halfway\ between}$ (m/s) | $v_{1/3\ way\ there}$ (m/s) | $\Delta v_{1/3\ way\ there}$ (m/s) | $v_{1/4\ way\ there}$ (m/s) | $\Delta v_{1/4\ way\ there}$ (m/s) |
|---|---|---|---|---|---|---|
| 21 | 304.6659 | 36.7498 | 304.6832 | 36.7519 | 304.7119 | 36.7553 |
| 22 | 309.5405 | 41.0965 | 309.5581 | 41.0988 | 309.5873 | 41.1027 |
| 23 | 314.5737 | 55.5035 | 314.5915 | 55.5066 | 314.6212 | 55.5118 |
| 24 | 313.3001 | 55.5947 | 313.3179 | 55.5978 | 313.3475 | 55.6031 |
| 25 | 309.5405 | 43.2039 | 309.5581 | 43.2064 | 309.5873 | 43.2105 |
| 28 | 309.5405 | 24.7632 | 309.5581 | 24.7646 | 309.5873 | 24.7670 |
| 29 | 307.0839 | 57.0402 | 307.1013 | 57.0435 | 307.1303 | 57.0488 |
| 2 | 309.5405 | 47.4190 | 309.5581 | 47.4217 | 309.5873 | 47.4262 |
| 7 | 325.1476 | 52.9027 | 325.1661 | 52.9057 | 325.1967 | 52.9107 |

*Table 8: Terminator Speeds for GQD and NAA.*

| Date(Nov/ Dec '06) | $v_{Halfway\ between}$ (m/s) | $\Delta v_{Halfway\ between}$ (m/s) | $v_{1/3\ way\ there}$ (m/s) | $\Delta v_{1/3\ way\ there}$ (m/s) | $v_{1/4\ way\ there}$ (m/s) | $\Delta v_{1/4\ way\ there}$ (m/s) |
|---|---|---|---|---|---|---|
| 21 | 265.1989 | 27.9660 | 265.2279 | 27.9690 | 266.0034 | 27.9690 |
| 22 | 265.9743 | 20.8490 | 266.0034 | 20.8513 | 265.2279 | 20.8513 |
| 23 | 265.1989 | 27.9659 | 265.2279 | 27.9689 | 263.6904 | 27.9689 |
| 24 | 263.6615 | 36.0979 | 263.6904 | 36.1019 | 260.6681 | 36.1019 |
| 25 | 260.6396 | 35.5931 | 260.6681 | 35.5970 | 259.1828 | 35.5970 |
| 28 | 259.1545 | 18.8510 | 259.1828 | 18.8531 | 259.1828 | 18.8531 |
| 29 | 259.1545 | 31.7325 | 259.1828 | 31.7360 | 259.9233 | 31.7360 |
| 2 | 259.8949 | 30.6502 | 259.9233 | 30.6536 | 262.9282 | 30.6536 |
| 7 | 262.8995 | 30.7164 | 262.9282 | 30.7197 | 266.0034 | 30.7197 |

*Table 9: Terminator Speeds for HWU and NAA*

APPENDIX 9:

Movement of Sunspot 10930 across the Sun's surface. [Gallagher 2002][23]

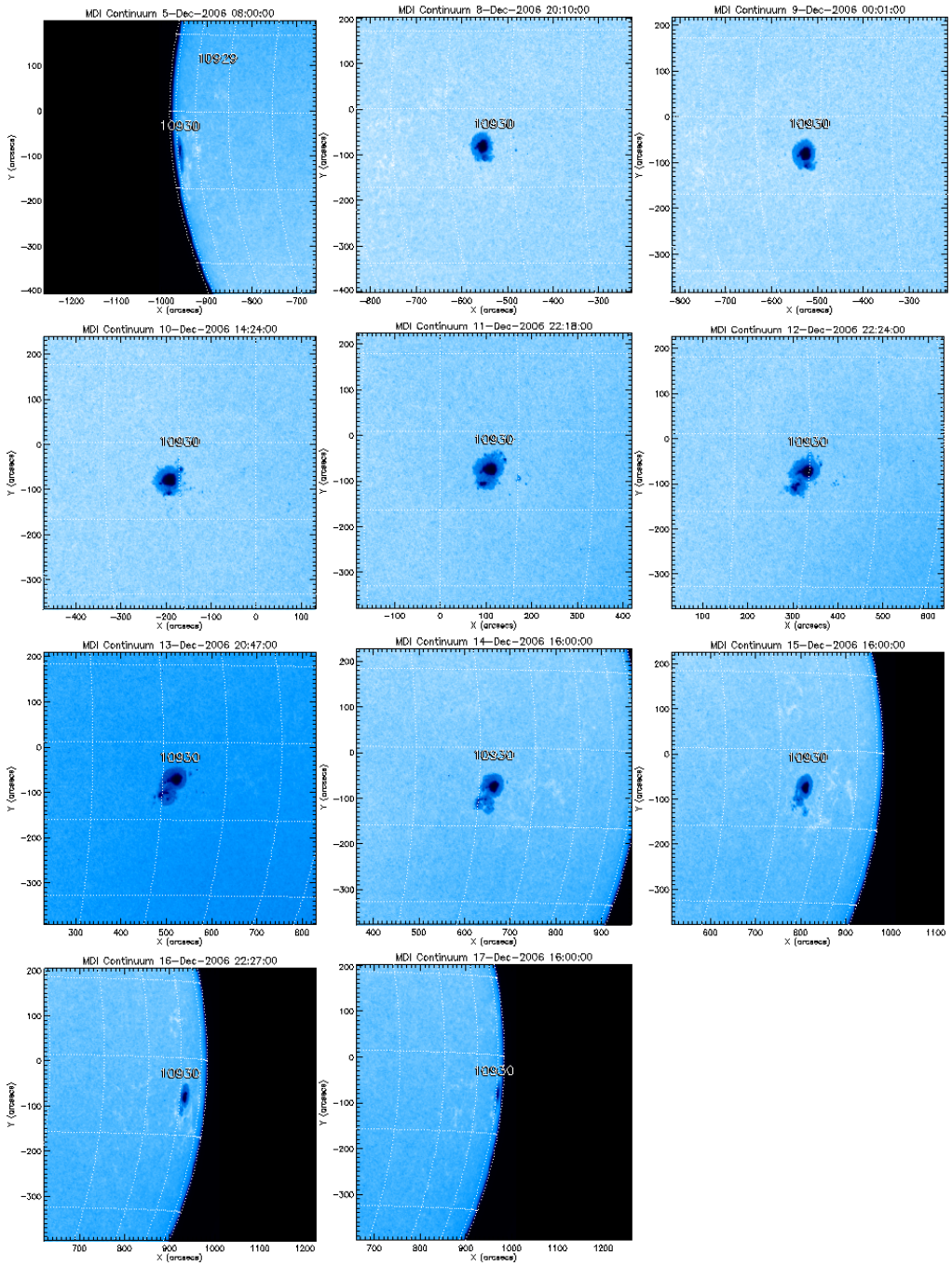


[23] http://www.solarmonitor.org